
COHERENT BEAM COMBINING OF FIBER AMPLIFIERS VIA LOCSET (POSTPRINT)

Angel Flores, et al.

10 July 2012

Technical Paper

APPROVED FOR PUBLIC RELEASE; DISTRIBUTION IS UNLIMITED.



AIR FORCE RESEARCH LABORATORY
Directed Energy Directorate
3550 Aberdeen Ave SE
AIR FORCE MATERIEL COMMAND
KIRTLAND AIR FORCE BASE, NM 87117-5776

REPORT DOCUMENTATION PAGE			<i>Form Approved</i> OMB No. 0704-0188	
Public reporting burden for this collection of information is estimated to average 1 hour per response, including the time for reviewing instructions, searching existing data sources, gathering and maintaining the data needed, and completing and reviewing this collection of information. Send comments regarding this burden estimate or any other aspect of this collection of information, including suggestions for reducing this burden to Department of Defense, Washington Headquarters Services, Directorate for Information Operations and Reports (0704-0188), 1215 Jefferson Davis Highway, Suite 1204, Arlington, VA 22202-4302. Respondents should be aware that notwithstanding any other provision of law, no person shall be subject to any penalty for failing to comply with a collection of information if it does not display a currently valid OMB control number. PLEASE DO NOT RETURN YOUR FORM TO THE ABOVE ADDRESS.				
1. REPORT DATE (DD-MM-YYYY) 10-07-2012		2. REPORT TYPE Technical Paper		3. DATES COVERED (From - To) 10 July 2012 - 10 July 2012
4. TITLE AND SUBTITLE Coherent Beam Combining of Fiber Amplifiers via LOCSET (Postprint)			5a. CONTRACT NUMBER	
			5b. GRANT NUMBER	
			5c. PROGRAM ELEMENT NUMBER	
6. AUTHOR(S) Angel Flores, Benjamin Pulford, Craig Robin, Chunte A. Lu, Thomas Shay			5d. PROJECT NUMBER	
			5e. TASK NUMBER	
			5f. WORK UNIT NUMBER D061	
7. PERFORMING ORGANIZATION NAME(S) AND ADDRESS(ES) Air Force Research Laboratory 3550 Aberdeen Ave SE Kirtland AFB, NM 87117-5776			8. PERFORMING ORGANIZATION REPORT NUMBER	
9. SPONSORING / MONITORING AGENCY NAME(S) AND ADDRESS(ES) Air Force Research Laboratory 3550 Aberdeen Ave SE Kirtland AFB, NM 87117-5776			10. SPONSOR/MONITOR'S ACRONYM(S) AFRL/RDLT	
			11. SPONSOR/MONITOR'S REPORT NUMBER(S) AFRL-RD-PS-TP-2015-0007	
12. DISTRIBUTION / AVAILABILITY STATEMENT Approved for public release: distribution unlimited. 377ABW-2012-1015; 24 July 2012.				
13. SUPPLEMENTARY NOTES Accepted for publication: A. Flores, B. Pulford, C. Robin, C. A. Lu, and T. M. Shay, Coherent Beam Combining of Fiber Amplifiers via LOCSET, in Coherent Laser Beam Combining (ed A. Brignon), Wiley-VCH, ISBN: 9783527411504, Chapter 2: 45-73 (2013). "Government Purpose Rights"				
14. ABSTRACT Fiber laser systems with a broad range of industrial [1], medical [2], and military [3] applications have evolved rapidly over the past decade. Generally, fiber lasers offer several advantages over conventional solid state and chemical lasers including: compactness, near diffraction limited beam quality, superior thermal-optical properties, and high optical to optical conversion efficiencies. Despite their advantages and brisk development, fiber lasers are still behind both chemical and bulk solid state lasers in terms of total output power. Currently, the intensity, and hence power available from single-mode optical fibers are limited by optical surface damage, thermal loads, and nonlinear optical effects.				
15. SUBJECT TERMS Thermal Loads, Fiber Lasers, Coherent Beam Combining, LOCSET				
16. SECURITY CLASSIFICATION OF:			17. LIMITATION OF ABSTRACT SAR	18. NUMBER OF PAGES 32
a. REPORT Unclassified	b. ABSTRACT Unclassified	c. THIS PAGE Unclassified		
			19b. TELEPHONE NUMBER (include area code) 505-846-4517	

Coherent Beam Combining of Fiber Amplifiers via LOCSET

Angel Flores, Benjamin Pulford, Craig Robin, Chunte A. Lu, and Thomas M. Shay
Air Force Research Laboratory, Directed Energy Directorate, 3550 Aberdeen Avenue SE,
Kirtland Air Force Base, New Mexico 87117, USA

1. Introduction

Fiber laser systems with a broad range of industrial [1], medical [2], and military [3] applications have evolved rapidly over the past decade. Generally, fiber lasers offer several advantages over conventional solid state and chemical lasers including: compactness, near diffraction limited beam quality, superior thermal-optical properties, and high optical to optical conversion efficiencies. Despite their advantages and brisk development, fiber lasers are still behind both chemical and bulk solid state lasers in terms of total output power. Currently, the intensity, and hence power available from single-mode optical fibers are limited by optical surface damage, thermal loads, and nonlinear optical effects.

Due to small core sizes and long amplifier lengths; high-power, single-mode fiber lasers are limited by the onset of (power-dependent) detrimental effects, such as stimulated Brillouin scattering (SBS) [4,5] and modal instabilities [6,7]. SBS is a third-order phase-matched nonlinear interaction that couples acoustic phonons to photons of the optical field and the associated backscattered Stokes light. Consequently, optical power is transferred from the laser field to the Stokes light; thus degrading amplification of the signal light and possibly damaging the fiber amplifier through pulsation. In addition to nonlinear effects, a recent phenomenon limiting power scaling of large mode area (LMA) fiber amplifiers has been modal instabilities; or the modal “hopping” of the fundamental mode (LP_{01}) into the next higher order mode (LP_{11}). A fundamental problem of LMA fibers is that they are inherently multi-mode. As a result, there have been recent reports of a sudden and dramatic loss in beam quality above a certain modal instability threshold [7]. Due to such constraints, single-mode fiber lasers do not meet requirements for future long-range directed energy (DE) applications. As a result, to scale overall power and brightness, beam combining techniques where multiple lasers are efficiently combined into a single output beam while maintaining high beam quality (and brightness) are being actively researched.

1.1 Beam Combination Architectures

The major beam combining techniques can be broadly categorized into incoherent [8] and coherent [9] beam combining approaches. A brief summary of the major beam combining approaches is presented in Table 1. In incoherent beam combining, an array of lasers are superimposed in the far field without control of the relative spectra or phases of the different elements. Such beam combining has been demonstrated at range (1.2 km) with powers up to 3 kW [10]. Similarly, in spectral beam combining (SBC), a separate class of incoherent beam combining, incoherent beams of different wavelengths are spatially overlapped (in the near field) to create a single beam of multiple colors. SBC has the advantage of not requiring active phase control or mutual temporal coherence of the individual beams. Although combined powers of 8 kW ($M^2 \sim 4$) have been reported [11], SBC channel scalability may be limited by the finite gain

bandwidth and beam quality (as a function of linewidth) sensitivity of the combining gratings [12].

Beam Combining Techniques	Advantages	Disadvantages	Combined Power
Coherent Beam Combining (Tiled Aperture)	<ul style="list-style-type: none"> - Atmospheric compensation possible - Fine electronic beam steering - N^2 irradiance scaling 	<ul style="list-style-type: none"> - Active phase control required - Low array fill factor limits PIB (50%-70%); dependent on number of array sub-apertures, sub-aperture packing, and optical fill of individual array sub-apertures 	<ul style="list-style-type: none"> - 1.4 kW w/ 16 elements [21] (single-frequency/AFRL) - 4 kW w/ 8 elements [22] (10 GHz, MIT-LL)
Coherent Beam Combining (Filled Aperture, DOE)	<ul style="list-style-type: none"> - Excellent beam quality - Power concentrated in single lobe 	<ul style="list-style-type: none"> - Active phase control required - Combining element power handling 	<ul style="list-style-type: none"> - 2 kW w/ 5 elements (10 GHz linewidth/ MIT-LL) [23]
Passive Beam Combination	<ul style="list-style-type: none"> - No active phase control 	<ul style="list-style-type: none"> - Limited scalability 	<ul style="list-style-type: none"> - 0.7 kW w/ 4 elements [24] (Lockheed-Aculight)
Spectral Beam Combining	<ul style="list-style-type: none"> - No active phase control required - Excellent beam quality - Power concentrated in single lobe 	<ul style="list-style-type: none"> - Scalability influenced by laser gain bandwidth - Beam quality sensitive to laser linewidth 	<ul style="list-style-type: none"> - 8 kW w/ 4 elements (Friedrich-Schiller Univ.) [11]
Incoherent Beam Combination	<ul style="list-style-type: none"> - Higher power from single amplifier (no SBS or linewidth limitations) - Simplicity in design 	<ul style="list-style-type: none"> - Steering optics required for each beam - Limited propagation range - Requires a large platform 	<ul style="list-style-type: none"> - 3 kW w/ 4 elements (NRL) [10]

Table 1. Brief summary of major beam combining architectures and techniques.

1.2 Active and Passive Coherent Beam Combining

In contrast, coherent beam combining (CBC) schemes require proper phase, frequency, and polarization relationships for efficient combination. CBC can be divided into techniques that use active or passive techniques to force coherence between all array elements. Active CBC uses electronic feedback to equalize and control the optical phase of the individual laser array elements, while passive CBC relies on self-phase locking via passive coupling mechanisms (ie., fiber ring [13] and Self-Fourier cavity [14]) to coherently combine multiple lasers. Despite bypassing complex phase controls required in active CBC, passive scaling to higher channel counts appear limited with maximal channel counts, N_{max} , of 10 to 12 elements predicted [15].

In comparison, active CBC with channel scalability of up to 64 elements has been reported [16] and channel counts up to 100 appear feasible [17]. Active CBC can be further divided into tiled aperture and filled aperture combining architectures. In tiled array formats, individual laser array

elements are combined (interfered) in the far field regime. Tiled array systems have several advantages such as fine electronic beam steering [18], potential N^2 irradiance scaling [19], distributed thermal load on final optics, and atmospheric turbulence compensation [20]. More importantly, tiled array systems are being investigated for extension to fiber phased array platforms and remote target phase locking. Nevertheless, tiled array systems are limited by non-uniform fill factors which contribute to far-field side lobes that limit the optical power in the central lobe. In general optimal closed packed hexagonal arrays of Gaussian filled circular sub-apertures predict power-in-the-central bucket values of $\sim 75\%$ [19]. With regard to tiled apertures, combined single-frequency and narrow-linewidth fiber arrays of 1.45 kW [21] and 4 kW [22], respectively, have been reported.

Contrary to tiled arrays, filled aperture techniques are based on near-field beam combining of laser array elements. Similar to utilizing a beam splitter in reverse, a beam combining optic is required to overlap the lasers in the near field. Filled aperture beam combination has the advantage of maintaining the near-diffraction limited beam quality of fiber lasers; with all power deposited into a single coherent beam. However, filled array systems require a combining element capable of managing the entire combined power. To date, combined powers of up to 2 kW [23] have been reported in filled array systems.

Regardless of the CBC architecture, active phase control of the array elements are required. As such several techniques have been developed for electronic phase control. In this chapter, we describe and detail coherent beam combining of fiber amplifiers via Locking of Optical Coherence by Single-Detector Electronic-Frequency Tagging (LOCSET) [17,21,29-30,33]. LOCSET is a novel approach to electronic phase locking that eliminates the need for a reference beam and requires a single-detector for full phase correction and beam combining. Herein we will discuss the theory of LOCSET operation and detail low-power LOCSET beam combining demonstrations of up to 32 elements with $\lambda/71$ average residual phase error. Moreover, high power kW scale CBC of conventional silica fiber and photonic crystal fiber amplifiers (PCF) via LOCSET phase locking is reported. Successful tiled array beam combination of sixteen single-frequency 100W lasers into a kilowatt class (1.4 kW) laser beam is presented. In addition, kW scale filled aperture CBC of novel SBS suppressive PCF amplifiers is detailed.

2. LOCSET

In order to coherently combine multiple lasers accurate control of the optical phase is required. Some of the more prominent methods of active phase control include heterodyne [25-26], Stochastic Parallel Gradient Descent (SPGD) [27-28], and LOCSET [17,21,29-30,33] phase locking techniques. In heterodyne phase locking, each optical channel phase locks to a common frequency shifted reference beam. While the scheme is noted for its simplicity and excellent phase error performance ($\lambda/80$ residual phase fluctuation for two element beam combining reported [31]), the method is hindered by the detector array arrangement (N detectors needed to combine N beams) and its common reference beam requirement. Here the elimination of the reference element would terminate the coherent beam combination.

In contrast, SPGD requires a single-detector for CBC. During operation a random optical phase perturbation is applied in parallel to each phase controlled beam. Then an intensity based metric algorithm is implemented to optimally combine (interfere) the beams in the near or far field.

Notably, SPGD can be used for additional higher order wavefront controls and 48 channel phase locking with $\lambda/30$ residual phase error [32] has been demonstrated. Nonetheless, SPGD may be limited by the inverse relationship between SPGD control loop bandwidth (BW_{SPGD}) and number of combined beams N ($BW_{SPGD} \propto 1/N$) [33].

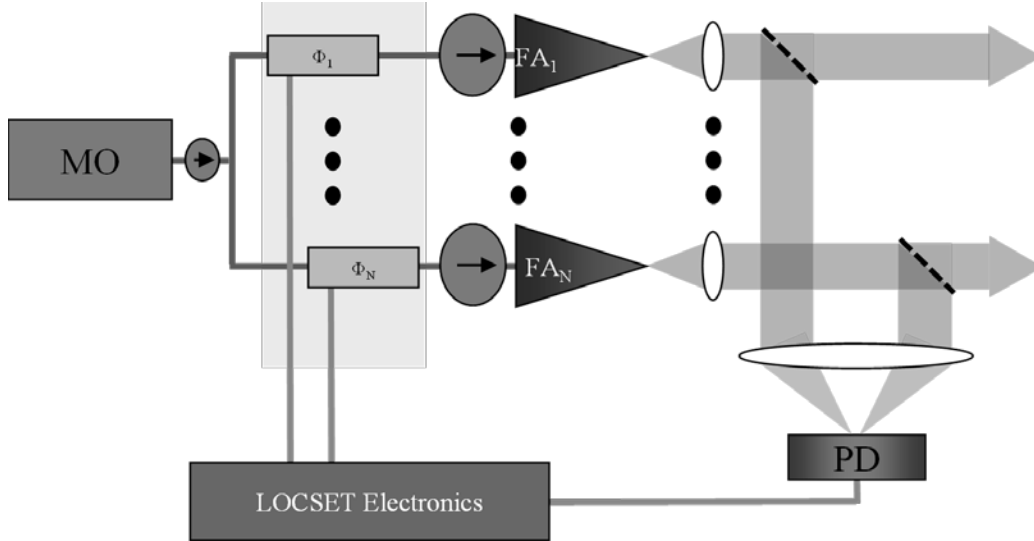


Figure 1. General LOCSET active CBC schematic. MO: Master Oscillator. PD: photodiode.

Similar to SPGD, LOCSET utilizes a single photodetector for active phase locking. However, LOCSET is not a stochastic, intensity based process. Based on coherent RF demodulation, LOCSET electronics is capable of independently determining an error signal proportional to the optical phase difference of each beam measured with respect to every other beam in the array. Although LOCSET can only apply piston phase corrections, its excellent phase error performance at high channel counts (and high bandwidth) make it attractive for active CBC.

The LOCSET system, as shown in Figure 1, typically employs a master oscillator power amplifier (MOPA) configuration where a narrow linewidth laser is split N ways and seeds an array of fiber amplifiers (FA). Prior to amplification each of the N beams passes through a phase modulator allowing the LOCSET control electronics the ability to apply piston phase corrections to each beam in the system for efficient combining. Each of the N beams is then amplified, collimated, and launched from the exit aperture of the system. Here the sampled light from a partial reflector is overlapped (interfered) onto a single photodetector that feeds into the LOCSET control electronics. To achieve optimal beam combination each of the N beams is “tagged” with a small amplitude phase dither at a unique RF frequency. These phase dithers are then measured at the photodetector as an intensity interference beat note that contains the phase information needed for coherent beam combining. Subsequently, in the next sections we detail the general LOCSET theory and operation.

2.1 LOCSET Theory

There are two operational configurations of LOCSET: self-referenced and self-synchronous phase locking [29,33]. In self-referenced phase locking $N-1$ beams are tagged with a unique RF phase dither which is used to demodulate the phase difference of a single beam with respect to all other beams in the system. Here the remaining un-modulated beam is used as a reference for

each of the RF phase modulated elements to minimize the phase difference between itself and the reference. It is important to note that a reference beam is not required in LOCSET. As we will show, if the amplitude of the un-modulated reference beam is set to zero, the expression for the phase error signal remains valid. This technique, known as self-synchronous LOCSET, determines the phase difference between itself and all other channels and applies the appropriate phase corrections. Because each channel is working towards minimizing the phase difference between itself and all other beams, the phase difference between the beams will converge to zero and establish optimal beam combination.

2.2 Self-Referenced LOCSET

In self-referenced LOCSET, there are $N-1$ phase modulated beams, $E_i(t)$, and a single-un-modulated reference beam, $E_u(t)$, expressed as:

$$E_u(t) = E_{u0} \cos(\omega_L t + \phi_u(t)), \quad (1)$$

$$E_i(t) = E_{i0} \cos(\omega_L t + \phi_i(t) + \beta_i \sin(\omega_i t)). \quad (2)$$

Here E_{u0} and E_{i0} are the field amplitudes of the un-modulated and phase modulated beams respectively. The angular laser frequency is ω_L , and $\phi_u(t)$ and $\phi_i(t)$ are the time varying phase states of the un-modulated and modulated beams, respectively. We note that since $\phi_u(t)$ and $\phi_i(t)$ have much slower variations than both the optical laser and RF modulation frequencies; they will be treated as constants. For the phase modulated beams, the third added term ($\beta_i \sin(\omega_i t)$) represents an applied sinusoidal phase modulation with amplitude β_i and RF modulation frequency ω_i . In practice, to minimize residual phase errors the RF modulation amplitude is kept on the order of $1/10^{\text{th}}$ of a radian or approximately $1/60^{\text{th}}$ of the optical wavelength ($\lambda/60$).

2.2.1 Photocurrent Signal

A basic LOCSET signal processing diagram is presented in Figure 2, where the overlapped beams on the photodetector produce a combined electric field, $E_T(t)$ represented as

$$E_T(t) = E_u(t) + \sum_{i=1}^{N-1} E_i(t), \quad (3)$$

with the individual fields represented by Eqs. (1) and (2), respectively. Accordingly, the electric field produces a photocurrent at the detector ($i_{PD}(t)$) defined as

$$i_{PD}(t) = R_{PD} \cdot A \cdot \frac{1}{2} \cdot \left(\frac{\epsilon_o}{\mu_o} \right)^{1/2} \cdot E_T^2(t), \quad (4)$$

where R_{PD} is the responsivity of the photodetector, and A is the active area of the photodetector. Next, substituting Eq. (3) into Eq. (4) with arbitrary summation indices j and k yields

$$i_{PD}(t) = R_{PD} \cdot A \cdot \frac{1}{2} \cdot \left(\frac{\epsilon_o}{\mu_o} \right)^{\frac{1}{2}} \cdot \left(E_u^2(t) + 2 \cdot E_u(t) \cdot \sum_{j=1}^{N-1} E_j(t) + \left(\sum_{j=1}^{N-1} E_j(t) \right) \left(\sum_{j=1}^{N-1} E_k(t) \right) \right). \quad (5)$$

Noticeably, the photocurrent in Eq. (5) can be divided into 3 components: a photocurrent due to un-modulated reference beam ($i_u(t)$), a photocurrent due to the un-modulated reference beam interfering with the phase modulated beams ($i_{uj}(t)$), and a photocurrent due to interference of each phase modulated beam with all other modulated beams ($i_{jk}(t)$), or

$$i_{PD}(t) = i_u(t) + i_{uj}(t) + i_{jk}(t) \quad . \quad (6)$$

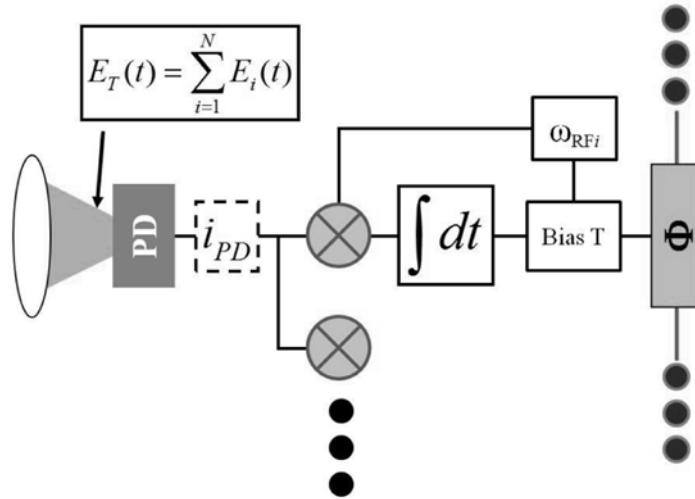


Figure 2. Basic LOCSET signal processing diagram. The phase modulated beams are combined and incident on the photodetector. The photocurrent is then mixed with a unique RF frequency and a phase error signal is generated via integration. The error signal and RF phase dither are then applied to a phase modulator keeping the i^{th} beam in phase with all other beams. An identical control loop is applied to all N , or $N-1$, channels.

A complete expression for the generated photocurrent can be derived by substituting Eqs. (1) and (2) into Eq. (5). This expression can then be partitioned into the three photocurrent components. For example, the photocurrent due to the un-modulated reference beam is

$$i_u(t) = \frac{R_{PD} \cdot P_u}{2} (1 + \cos(2\omega_L t + 2\phi_u)) \approx \frac{R_{PD} \cdot P_u}{2}, \quad (7)$$

where P_u is the optical power of the un-modulated beam and the terms oscillating at the laser frequency are neglected (cannot be resolved by photodetector). Thus, this photocurrent contributes a DC bias to the total current. Similarly, the photocurrent due to un-modulated beam interfering with the modulated beams, after substitution, yields

$$i_{uj}(t) = R_{PD} \cdot P_u^{\frac{1}{2}} \cdot \sum_{j=1}^{N-1} P_j^{\frac{1}{2}} \cdot \left(\cos(\phi_u - \phi_j) \cos(\beta_j \sin(\omega_j t)) + \sin(\phi_u - \phi_j) \sin(\beta_j \sin(\omega_j t)) \right), \quad (8)$$

and can be simplified through Fourier series expansion as follows

$$i_{uj}(t) = R_{PD} \cdot P_u^{1/2} \cdot \sum_{j=1}^{N-1} P_j^{1/2} \cdot \left(\begin{array}{l} \cos(\phi_u - \phi_j) \left(J_o(\beta_j) + 2 \sum_{n=1}^{\infty} J_{2n}(\beta_j) \cdot \cos(2n \cdot \omega_j t) \right) \\ + \sin(\phi_u - \phi_j) \left(2 \sum_{n=1}^{\infty} J_{2n-1}(\beta_j) \cdot \sin((2n-1) \cdot \omega_j t) \right) \end{array} \right), \quad (9)$$

where J_n is a Bessel function of the first kind of order n . We note that the second term in the sum of Eq. (9) is proportional to the sine of the phase difference between the un-modulated and modulated reference beam ($\sin(\phi_u - \phi_j)$). Notably, this term is a characteristic error signal where minimizing the sinusoidal phase difference equalizes the individual phases for optimal phase locking.

The final photocurrent term quantifies the interference of each phase modulated beam with the set of other phase modulated elements. Here after utilizing several trigonometric identities, Fourier series expansions and neglecting laser frequency oscillation, the photocurrent can be expressed as [33]:

$$i_{jk}(t) = \frac{R_{PD}}{2} \cdot \sum_{k=1}^{N-1} P_k^{1/2} \cdot \sum_{j=1}^{N-1} P_j^{1/2} \cdot \left(\begin{array}{l} \left(\cos(\phi_k - \phi_j) \left(J_o(\beta_k) + 2 \sum_{n_k=1}^{\infty} J_{2n_k}(\beta_k) \cdot \cos(2n_k \cdot \omega_k t) \right) \right) \\ \cdot \left(J_o(\beta_j) + 2 \sum_{n_j=1}^{\infty} J_{2n_j}(\beta_j) \cdot \cos(2n_j \cdot \omega_j t) \right) \\ - \left(\sin(\phi_k - \phi_j) \left(2 \sum_{n_k=1}^{\infty} J_{2n_k-1}(\beta_k) \cdot \sin((2n_k-1) \cdot \omega_k t) \right) \right) \\ \cdot \left(J_o(\beta_j) + 2 \sum_{n_j=1}^{\infty} J_{2n_j}(\beta_j) \cdot \cos(2n_j \cdot \omega_j t) \right) \\ + \left(\sin(\phi_k - \phi_j) \left(J_o(\beta_k) + 2 \sum_{n_k=1}^{\infty} J_{2n_k}(\beta_k) \cdot \cos(2n_k \cdot \omega_k t) \right) \right) \\ \cdot \left(2 \sum_{n_j=1}^{\infty} J_{2n_j-1}(\beta_j) \cdot \sin((2n_j-1) \cdot \omega_j t) \right) \\ + \left(\cos(\phi_k - \phi_j) \left(2 \sum_{n_k=1}^{\infty} J_{2n_k-1}(\beta_k) \cdot \cos((2n_k-1) \cdot \omega_k t) \right) \right) \\ \cdot \left(2 \sum_{n_j=1}^{\infty} J_{2n_j-1}(\beta_j) \cdot \cos((2n_j-1) \cdot \omega_j t) \right) \end{array} \right). \quad (10)$$

Once again, characteristic phase error signals proportional to the sinusoidal phase difference between the k^{th} and j^{th} modulated beams are generated ($\sin(\phi_k - \phi_j)$) allowing for ideal phase optimization.

2.2.2 LOCSET Demodulation

Once the combined interference signal reaches the photodetector, demodulation of the phase error signal for each of the modulated beams occurs, as shown in Figure 2. Schematically this is done via individual and independent control loops acting on each of the phase modulated channels. Although each control loop channel performs identical operations, each channel is distinguished by its unique RF modulation frequency, ω_i . To that end, the coherent demodulation process involves multiplying (mixing) the sampled photocurrent with an RF demodulation signal ($\sin(\omega_c t)$), and integrating over time τ . The subsequent RF demodulation can be expressed as

$$S_x = \frac{1}{\tau} \int_0^{\tau} i_{PD}(t) \cdot \sin(\omega_c t) dt. \quad (11)$$

Here ω_c represents the control loop demodulation frequency of the x^{th} LOCSET channel and S_x represents the phase error correction signal of the x^{th} modulated beam. Particularly, the demodulation frequency for each channel is chosen to equal that specific channel's RF phase dither frequency ($\omega_c = \omega_i = \omega_x$). In addition, the integration time is chosen such that the LOCSET control loop can isolate the phase error signal for all modulated beams (j and k), while remain short enough to effectively cancel the phase disturbances of the system:

$$\tau \gg \frac{2\pi}{|\omega_j - \omega_k|}, \quad (12)$$

Similar to the photocurrent signal the error signal can be divided into three components due to the interaction of the un-modulated beam, the un-modulated beam and all other phase modulated elements, and interference of each phase modulated beam with all other modulated beams or

$$S_x = S_u + S_{xu} + S_{xj}. \quad (13)$$

As such, to resolve the self-reference LOCSET phase error signal, Eqs. (7), (9) and (10) can be substituted into Eqs. (11) and (13). The first term S_u , due to the presence of the un-modulated beam is zero since there are no interference terms in Eq. (7):

$$S_u = \frac{R_{PD} \cdot P_u}{2\tau} \int_0^{\tau} \sin(\omega_x \cdot t) dt = \frac{R_{PD} \cdot P_u}{2} \left(\frac{1}{\omega_x \cdot \tau} - \frac{\cos \omega_x}{\omega_x \cdot \tau} \right) \approx 0 \quad (14)$$

Because there are no time varying contributions due solely to the presence of the un-modulated beam, this is expected. Next, by substituting Eq. (9) into Eq. (11), the second term due to interference of the un-modulated beam with the x^{th} phase modulated beam can be expressed as

$$S_{xu} = R_{PD} \cdot P_u^{1/2} \cdot P_x^{1/2} \cdot J_1(\beta_x) \cdot \sin(\phi_u - \phi_x), \quad (15)$$

where the remaining sinusoidal phase difference terms can be neglected due to the aforementioned long integration time, τ , (these integrals converge to zero [33]). In addition, Bessel functions beyond the second order were neglected as they evaluate near zero for the small modulation depths (β) imposed in LOCSET [33].

Subsequently, the last signal term is derived from the interference of the x^{th} modulated beam with all other phase modulated beams ($j \neq x$), S_{xj} . Eq. (10) is inserted into Eq. (11) with Bessel functions beyond the second order being neglected. Unfortunately, this yields an unwieldy solution due to the matrix of optical beam interactions involved. A complete analysis of this error signal derivation can be found in the literature where the following expression was obtained [33]

$$S_{xj} = R_{PD} \cdot P_x^{1/2} \cdot J_1(\beta_x) \cdot \frac{1}{2} \sum_{\substack{j=1 \\ j \neq x}}^{N-1} P_j^{1/2} J_0(\beta_j) \sin(\phi_j - \phi_x). \quad (16)$$

Here we note that, S_{xj} adds to the overall robustness of the LOCSET system. Differing from schemes where the phase error signal is governed by the independent interaction of each phase controlled beam with a common reference beam, LOCSET adds a measurement signal proportional to the sum of the phase difference of each beam with respect to all other beams in the system. Consequently, if the reference beam is lost, the LOCSET system continues to phase lock the remaining beams with graceful degradation. After deriving the individual phase error terms a complete representation of the Self-Referenced LOCSET phase error signal can be determined according to Eqs. (13), (14) and (15) [33],

$$S_{SRx} = R_{PD} \cdot P_x^{1/2} \cdot J_1(\beta_x) \left(P_u^{1/2} \sin(\phi_u - \phi_x) + \frac{1}{2} \sum_{\substack{j=1 \\ j \neq x}}^{N-1} P_j^{1/2} J_0(\beta_j) \sin(\phi_j - \phi_x) \right). \quad (17)$$

Fittingly, the phase error signal changes with slow variations in the optical phases of the combined beams. Due to the sinusoidal terms as long as the phase difference between each combined beam is zero, S_{SRx} is also zero. If the x^{th} beam drifts out of phase with the rest of the system, the phase error signal will be nonzero and carry a sign (\pm) indicating the phase drift direction. An error correction signal is then applied to the x^{th} beam (through external phase modulators) to minimize S_{SRx} and return the system to optimal phase locking. Likewise, independent LOCSET control loops for each additional phase modulated element ensures constant phase locking for all laser array elements.

2.3 Self-Synchronous LOCSET

It is important to note an un-modulated reference beam is not necessary for LOCSET operation. Referring back to self-referenced LOCSET and Eq. (17), only the first term inside the parenthesis is influenced by the un-modulated reference beam ($P_u^{1/2}$). Thus, by setting the un-modulated reference beam to zero ($P_u = 0$), we obtain the following phase error expression for self-synchronous LOCSET

$$S_{SSx} = R_{PD} \cdot P_x^{1/2} \cdot J_1(\beta_x) \cdot \frac{1}{2} \sum_{\substack{j=1 \\ j \neq x}}^{N-1} P_j^{1/2} J_0(\beta_j) \sin(\phi_j - \phi_x). \quad (18)$$

Appreciably, LOCSET is capable of operating without a reference beam. Because it measures the relative phase error of a single beam with respect to every other beam in the system, the phase information of a given beam is known with respect to all others. Thus, a reference beam is

no longer required. Similarly, the independent LOCSET control loops ensure persistent phase locking through minimization of the individual error signals, S_{SS_x} .

3. LOCSET Phase Error and Channel Scalability

Scalability to high channel counts and excellent phase error performance are critical parameters for any active CBC system. Towards that end, LOCSET has exhibited outstanding phase error performance with little degradation in residual phase error as we scale to higher channel counts. Such performance is vital for CBC, where a phase error dependent efficiency degradation, η_ϕ , is inherent [34]

$$\eta_\phi \approx 1 - \Delta\phi_{rms}^2 . \quad (19)$$

Hence, a residual phase error, $\Delta\phi_{rms}$, of $\lambda/15$ results in a prohibitive drop in efficiency (18%); while a $\lambda/60$ phase error contributes a negligible loss in efficiency (<1%). As such to characterize LOCSET's beam combining performance detailed low power multi-beam CBC and phase error analysis of 2, 16, and 32 lasers was performed [33].

3.1 LOCSET beam combining and phase error analysis

The general LOCSET experimental arrangement for coherent beam combining with diagnostic phase error analysis (in-phase (I) and quadrature (Q) processing [9,33,35-36]), is depicted in Figure 3. The setup is based on a MOPA arrangement with light from the master oscillator split $N+1$ ways with N (or $N-1$) phase modulated laser beams. The remaining beam (top of Figure 3), is coupled to an acousto-optic modulator (AOM) where the light undergoes a fixed frequency shift ($\nu_{RF} = 80\text{MHz}$). Here the frequency shifted beam is used as a phase stable reference for the phase error measurements. The combined output beam is then sampled with a 10% wedge, where the sampled light incident on a photodetector provides feedback to the LOCSET control electronics. After passing through another beam sampler (for intensity monitoring), the remaining light is coupled into a 2x2 fiber splitter/combiner where it is interfered with the frequency shifted reference beam.

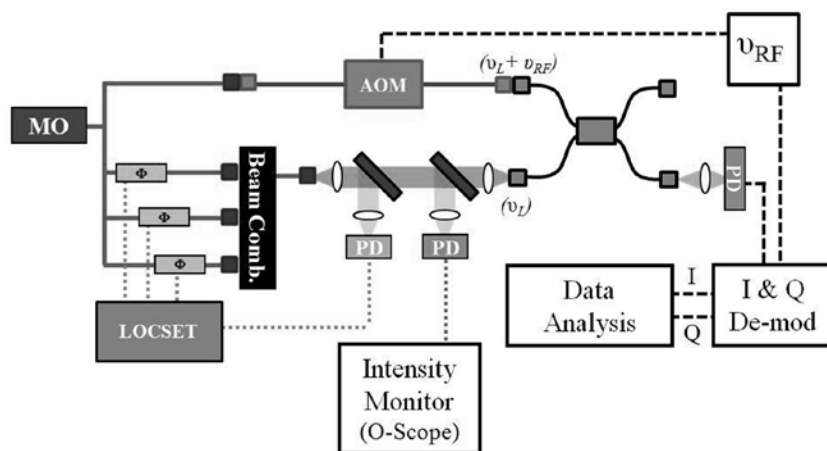


Figure 3: General LOCSET CBC experimental arrangement with in-phase (I) & quadrature (Q) demodulation for phase error analysis.

The combined output, a beat note caused by the different frequencies and phases of the beams, is incident on another photodetector which feeds into the I and Q data processing electronics. I and Q signals are then generated via coherent RF demodulation and measured as a function of time. Moreover, before initiating beam combining experiments the system background phase behavior due to external disturbances was quantified. By choosing a data sampling window less than or equal to 1 ms, the behavior of the frequency shifted reference beam was evaluated to be stable to within $\leq \lambda / 450$; when measured relative to any beam in the CBC system. Thus, establishing our phase error measurement resolution at $\sim \lambda / 450$ (~ 0.014 rad); significantly greater than the phase error tolerances needed to analyze LOCSET's phase error performance.

3.2 In-Phase and Quadrature Phase Error Analysis

The I & Q phase error analysis is based on the optical phase difference, $\Delta\phi$, between a phase stable reference laser and the combined laser beam. Referring to Figure 3, the AC photocurrent generated by the interfering lasers can be expressed as

$$i_{AC}(t) = \chi \cdot \cos(\Delta\omega \cdot t + \Delta\phi) , \quad (20)$$

where $\chi = R_{PD} \cdot A \cdot 2 \cdot Int_0$, is a constant term related to the optical intensity (Int_0), detector responsivity and active area. Likewise, $\Delta\omega$ is proportional to the difference in frequency between the combined output beam and the frequency shifted reference beam. Therefore after trigonometric expansion, the I and Q phase components can be described as:

$$i_{AC}(t) = I(\Delta\phi)\cos(\Delta\omega \cdot t) - Q(\Delta\phi)\sin(\Delta\omega \cdot t), \quad (21)$$

where

$$I(\Delta\phi) = \chi \cos(\Delta\phi) \quad (22)$$

$$Q(\Delta\phi) = \chi \sin(\Delta\phi). \quad (23)$$

Subsequently, the goal is to extract $I(\Delta\phi)$ and $Q(\Delta\phi)$ from Eq. (21) via coherent demodulation. We note that $I(\Delta\phi)$ and $Q(\Delta\phi)$ are the Fourier cosine and sine coefficients of $i_{AC}(t)$ at frequency $\Delta\omega$, respectively. These terms can be isolated by mixing $i_{AC}(t)$ with a sine or cosine demodulation signal at frequency $\Delta\omega$ and integrating over time T . The Fourier cosine component, a_c , can be expressed as

$$a_c = \frac{1}{T} \int_0^T i_{AC}(t) \cos(\Delta\omega \cdot t) dt, \quad (24)$$

where after substituting Eq. (21) into Eq. (24) and accounting for long integration times yields

$$a_c = \frac{I(\Delta\phi)}{T} \int_0^T \cos^2(\Delta\omega \cdot t) dt \approx \frac{I(\Delta\phi)}{2} . \quad (25)$$

Similarly, the Fourier sine component, a_s , can be extracted and represented as

$$a_s = -\frac{Q(\Delta\phi)}{2} . \quad (26)$$

Equations (25) and (26) provide us with measurable quantities that are proportional to the optical phase difference, $\Delta\phi$, between the reference field, E_R , and the field of interest E_i . Relating the ratio of a_s and a_c with Eqs. (23) and (24), we get an expression proportional to the tangent of the optical phase difference

$$\Delta\phi = \tan^{-1}\left(-\frac{a_s}{a_c}\right). \quad (27)$$

Therefore, by measuring $I(\Delta\phi)$ and $Q(\Delta\phi)$, or more accurately a_s and a_c , we can extract the optical phase difference as a slowly varying function of time. We note that due to asymptotic nature of the arctangent term, additional I and Q phase data unwrapping and processing are required [33]. Nevertheless, in-phase and quadrature phase analysis provides an adequate tool for LOCSET beam combining performance evaluation.

3.3 2-Channel Beam Combining

To highlight LOCSET's channel scalability and superior phase error performance, multi-channel LOCSET beam combining of 2, 16, and 32 channels was performed. The initial 2-channel experiment follows the general arrangement in Figure 3, with two low power beams (~ 2 mW) in the self-referenced LOCSET configuration. The beams were combined with a 2x2 fiber splitter (filled aperture scheme) and monitored for both intensity and phase behavior performance.

The subsequent intensity behavior of our 2 channel CBC system is shown in Figure 4. For the initial 2.5 seconds of data acquisition, the LOCSET electronics are off allowing the intensity to drift due to environmental disturbances. After, the LOCSET electronics were turned on to establish coherent combination of the 2 beams. While satisfactory beam combining is observed from Figure 4, it is difficult to extrapolate the phase behavior from the intensity data. For small phase errors ($< \lambda/25$), the phase behavior is lost in the measurement noise and the general interference expression used to extrapolate phase error may no longer be valid ($Int(\Delta\phi)/Int_0 = 2(1 + \cos(\Delta\phi))$). As a result, in-phase and quadrature phase analysis is performed.

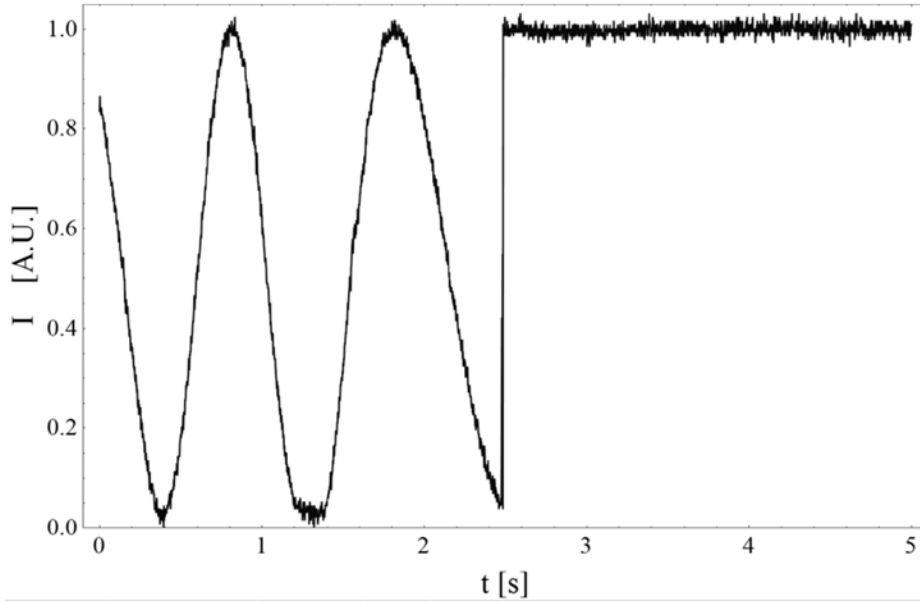


Figure 4: Time varying intensity of the 2 channel, LOCSET CBC system. LOCSET electronics remain off until 2.5 seconds into data acquisition [33].

We note that in addition to the phase noise of the combined beam, LOCSET control electronics contribute additional phase error that cannot be measured by the I and Q system. This is due to the RF phase dithers, with modulation depths, β_i , that are applied to each beam. In the current case, a 100 MHz RF phase dither with modulation depth of 0.094 rad ($\lambda/67$) is applied to the phase modulator. Therefore, to obtain the root-mean-square (RMS) phase error of the entire CBC system, we must determine the phase error of the RF sinusoidal dither of each beam ($\Delta\phi_{RF}$) and combine it with extracted the I and Q phase error ($\Delta\phi$). The RMS phase error contributed from the sinusoidal phase dither can be quantified as:

$$\Delta\phi_{RF} = \frac{\sqrt{2}}{2} \beta_{P-P}, \quad (28)$$

where β_{P-P} is the peak to peak amplitude of the time varying sinusoidal signal. Hence, for a phase modulation depth of 0.094 rad ($\lambda/67$), an RMS RF phase error of 0.067 rad is imparted. Further, since the sinusoidal RF phase modulation is well defined and the phase errors of the coherently combined beam vary arbitrarily (due to environmental disturbances), the two signals are effectively uncorrelated. Because the two signals are uncorrelated we can calculate the total RMS phase error signal as [33]

$$\Delta\phi_{RMS} = \sqrt{\Delta\phi^2 + \Delta\phi_{RF}^2}. \quad (29)$$

The ensuing average RMS phase error for two channel beam combination was measured as $\Delta\phi_{RMS} \approx \lambda / 66$ (0.095 rad), as shown in Figure 5 for multiple data sets. Notably, such phase error performance results in less than 1% drop in coherent combination efficiency. Though the data shown in Figure 5 was limited to a 5 minute data collection period, such beam combination performance and stability was observed for hours at a time, repeatedly.

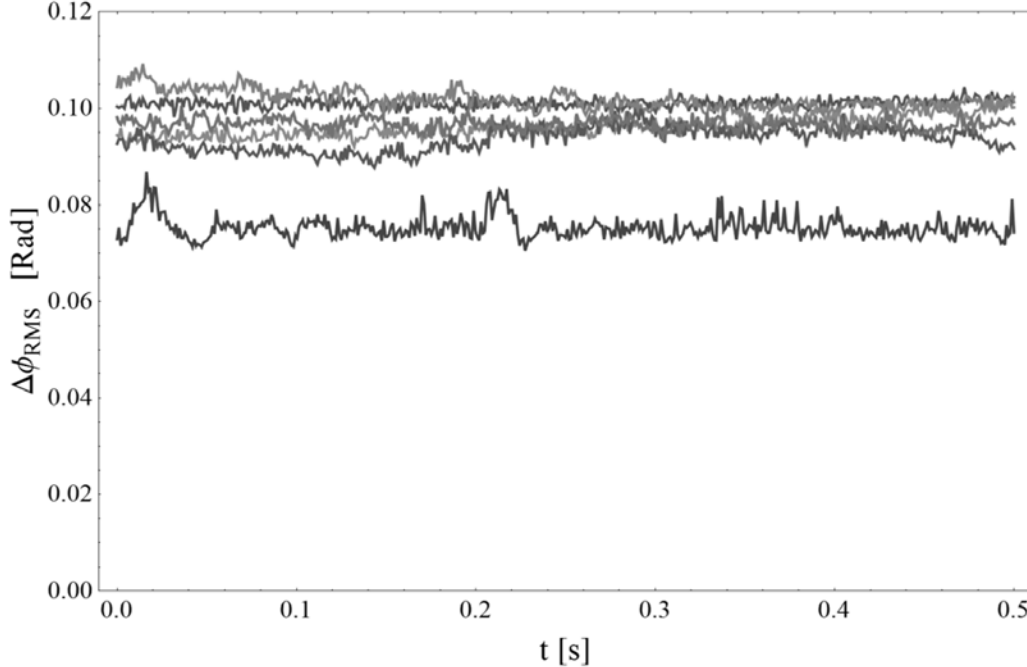


Figure 5: RMS phase error as a function of time for the 2 channel LOCSET CBC system. Multiple data sets, taken during a single run of the 2 channel system, were included to demonstrate consistency in beam combination performance. Average observed RMS phase error: $\sim\lambda/66$ [33].

3.4 16-Channel Beam Combining

The second LOCSET beam combination experiment combined 16 low power beams in the self-referenced LOCSET configuration. The experimental setup, shown in Figure 6, begins with a single MO split into 3 individual fiber channels. Two of the fiber channels are further cascaded into 16 individual fiber channels for coherent combination. These fiber channels are coupled into two 1×8 LiNbO₃ phase modulators, each converting a single input beam into 8 phase controllable optical channels for a total of 16 beams. The outputs of each 1×8 LiNbO₃ module are then recombined via a passive 1×8 LiNbO₃ fiber splitter/combiner, combining eight beams into one. The ensuing two beams, each consisting of 8 individual phase modulated beams, propagate in free space and combine at the interface of a 50/50 beam splitter in a filled aperture format. The remaining beam, as before, is frequency shifted via an AOM and used as a reference beam for I & Q phase error measurements. After, time varying intensity measurements of the final combined beam were recorded with a fast photodiode, as shown in Figure 7.

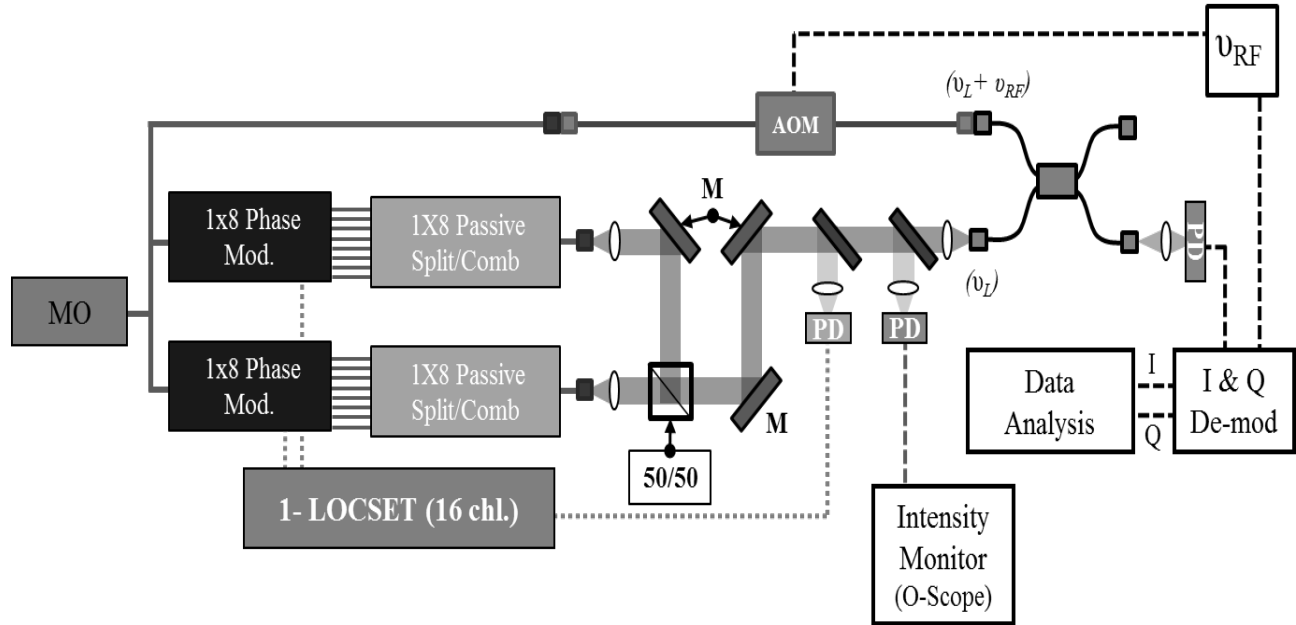


Figure 6: Experimental setup of a filled aperture 16 channel LOCSET CBC system. M: Mirror. 50/50: 50% reflective/transmissive beam splitter.

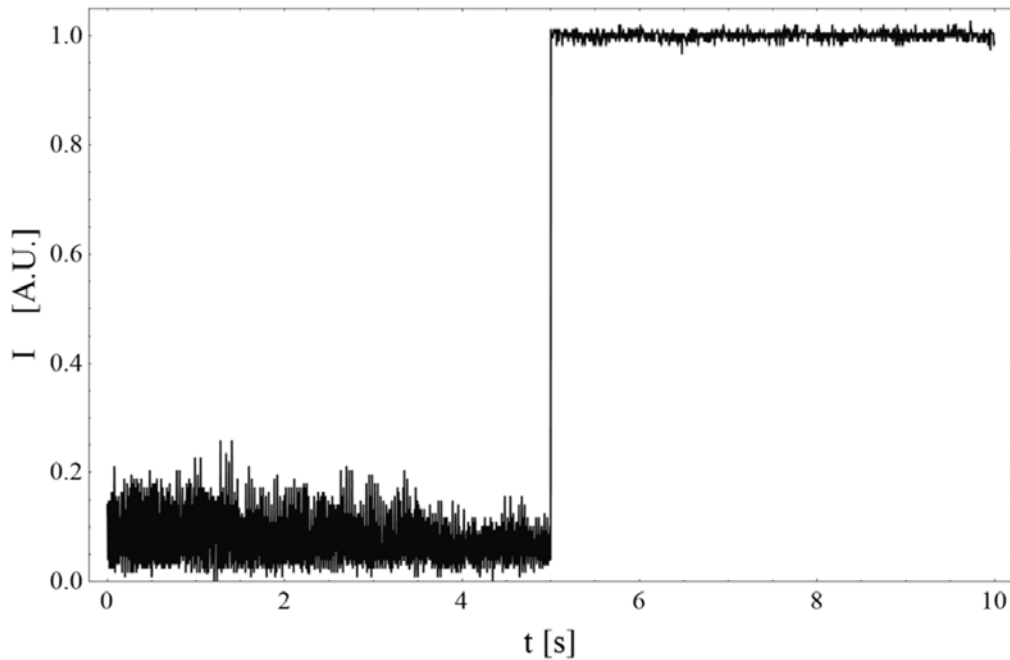


Figure 7: Time varying intensity of the 16 channel LOCSET CBC system. LOCSET electronics remain on for the entire data acquisition time. LOCSET return signal photodetector blocked for the first 5 seconds of the data acquisition. After 5 seconds the LOCSET detector was unblocked allowing the system to phase lock [33].

Figure 7 illustrates the intensity disparity of the 16 channel LOCSET system when the system is locked and unlocked. When the LOCSET detector is blocked, the intensity of the combined output beam fluctuates due to the oscillating phase behavior of the 15 modulated beams. However, when the LOCSET detector is active the intensity is stabilized at peak intensity (optimal beam combination). Subsequently, in-phase and quadrature phase error analysis was

performed to quantify the RMS phase behavior. The ensuing data shown in Figure 8 represents the RMS phase error as a function of time for the 16 channel LOCSET system. Here we observe rapid phase fluctuations due to the 2π phase reset voltages. In order to protect the phase modulators from voltage overloading the phase is unwrapped continuously at $2N\pi$ intervals ($N = 1$ for the current experiments). Therefore, 15 phase modulators are randomly resetting or unwrapping according to the operating environment and thermal/vibrational disturbances. Nevertheless, the average RMS phase error performance of the 16 channel LOCSET CBC experiment was excellent, $\lambda/62$ (0.1 rad).

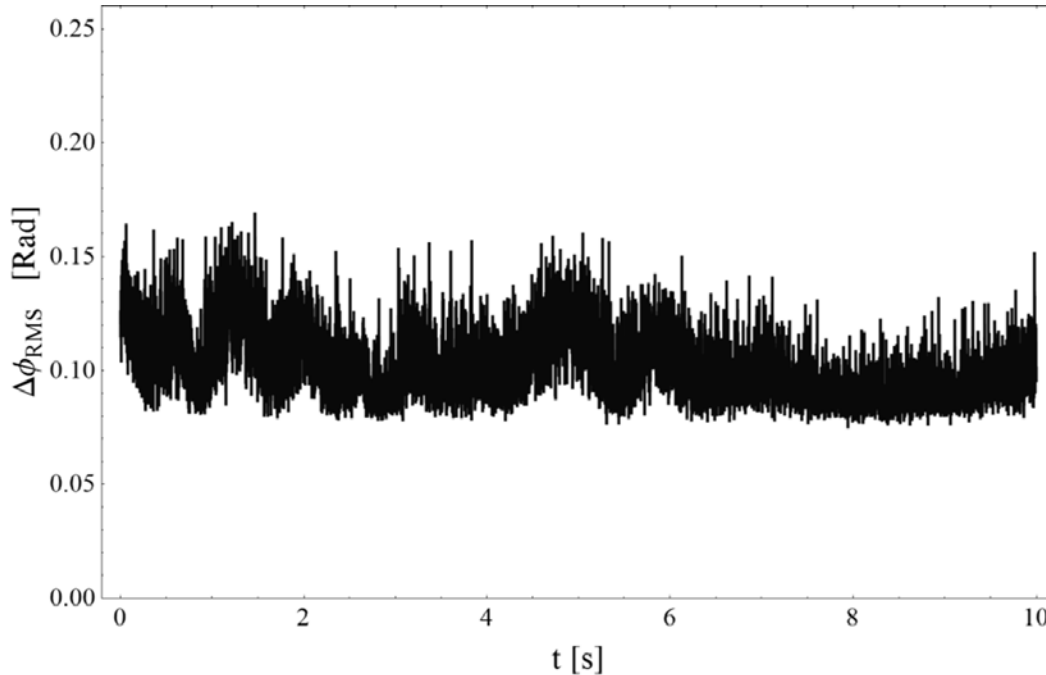


Figure 8: Measured RMS phase error as a function of time for the 16 channel, LOCSET CBC experiment. RMS values calculated over a time period of 1ms. Average observed RMS phase error for 16 channel system: $\sim\lambda/62$ (0.1 rad) [33].

3.5 32-Channel Beam Combining

The third low power beam combining experiment, depicted in Figure 9, was a 32 channel self-referenced LOCSET demonstration. The experimental arrangement remains similar to the 16 channel setup, except the MO is split 5 ways with four of the channels further cascaded into 32 channels using 1×8 LiNbO₃ phase modulators. The fifth channel is used as a frequency shifted reference beam. The outputs of the LiNbO₃ modules are then recombined via passive LiNbO₃ fiber splitters. The ensuing 4 combined beams, each consisting of 8 phase modulated beams propagate in free space and combine via a binary splitter tree (filled aperture configuration). The binary tree consists of three 50/50 beam splitters and combines the four free-space beams into a single coherent beam. The final beam is then processed via the same optical setup providing the LOCSET error signal and beam combination performance measures.

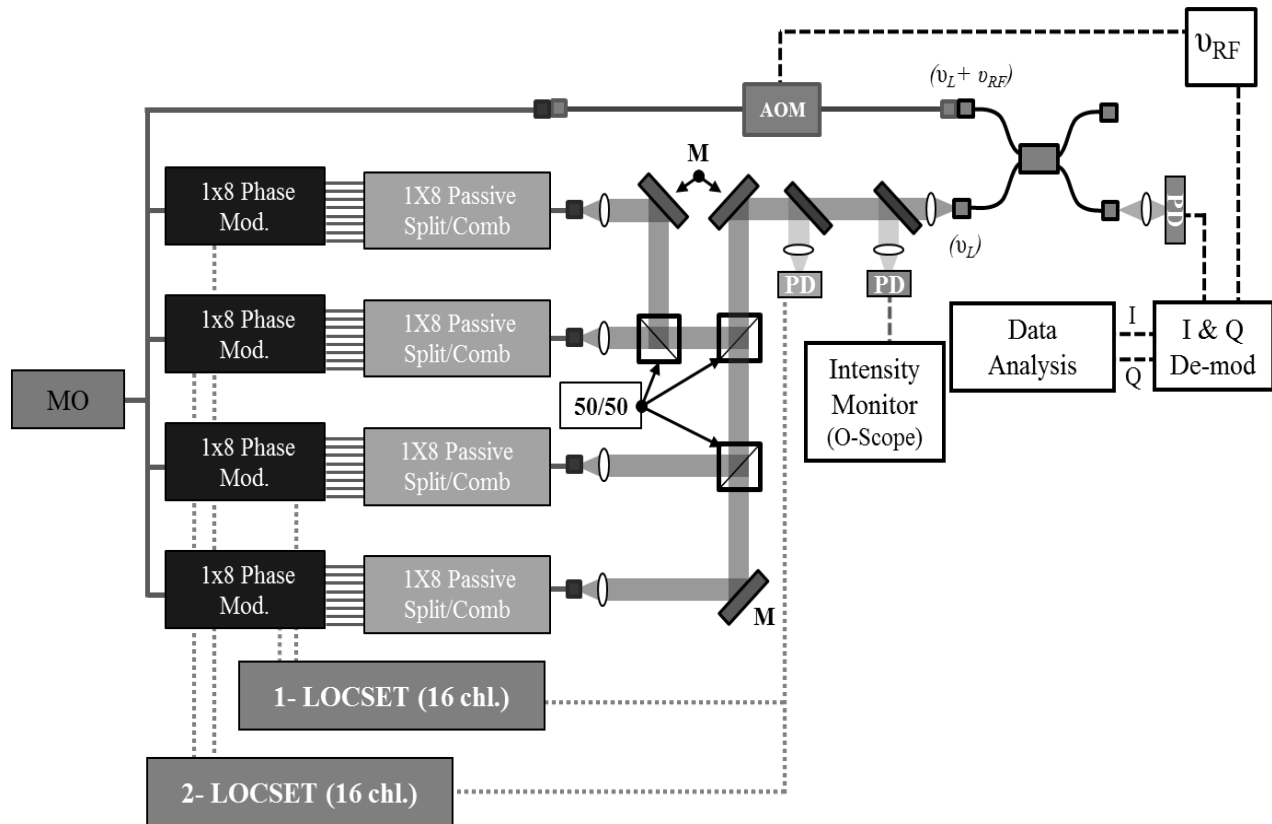


Figure 9: Experimental setup of a 32 channel LOCSET CBC system [33].

The time varying intensity of the 32 channel LOCSET beam combining system is shown in Figure 10. Once again successful coherent combination is observed with stable peak intensity. The I & Q phase error data shown in Figure 11 represents the RMS phase error of the 32 channel combined beam as a function of time. Yet again, the presence of random 2π phase resets in each of the 31 phase controlled beams contributes to the fluctuating phase errors. Despite these fluctuations the average RMS phase error of the 32 channel coherently combined beam was approximately $\lambda/71$ (~ 0.09 rad). A promising result, but more importantly no phase error degradation was detected when scaling from 2 channels to 32 channels, as expected from previous simulations [17]. As such, LOCSET appears readily scalable to more than 100 elements as the RMS phase error appears to be independent of the number of array elements in the system.

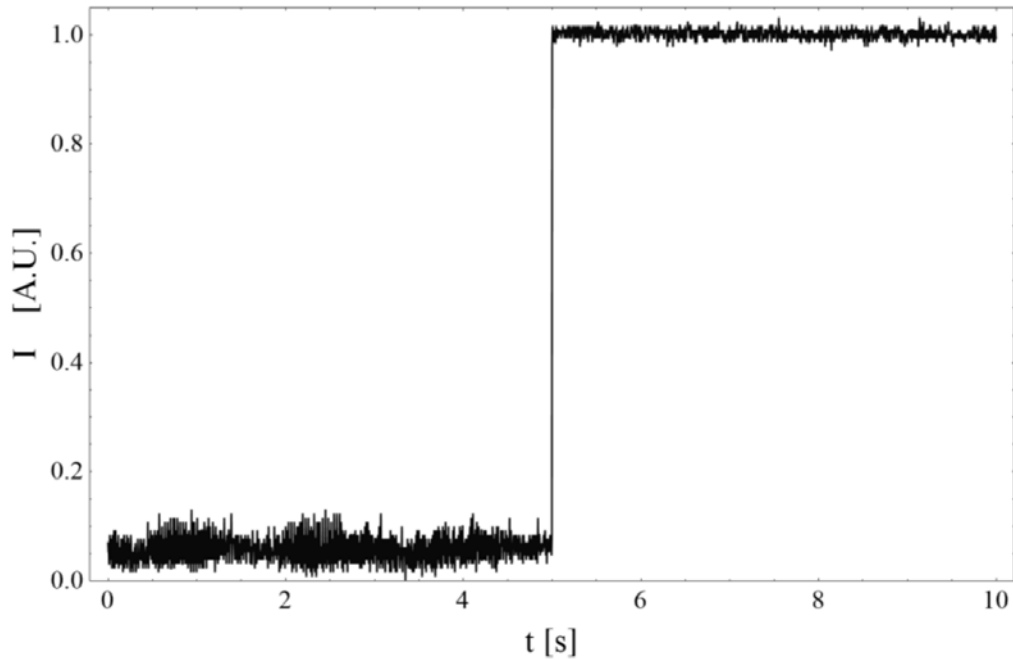


Figure 10: Time varying intensity of the 32 channel LOCSET CBC system [33].

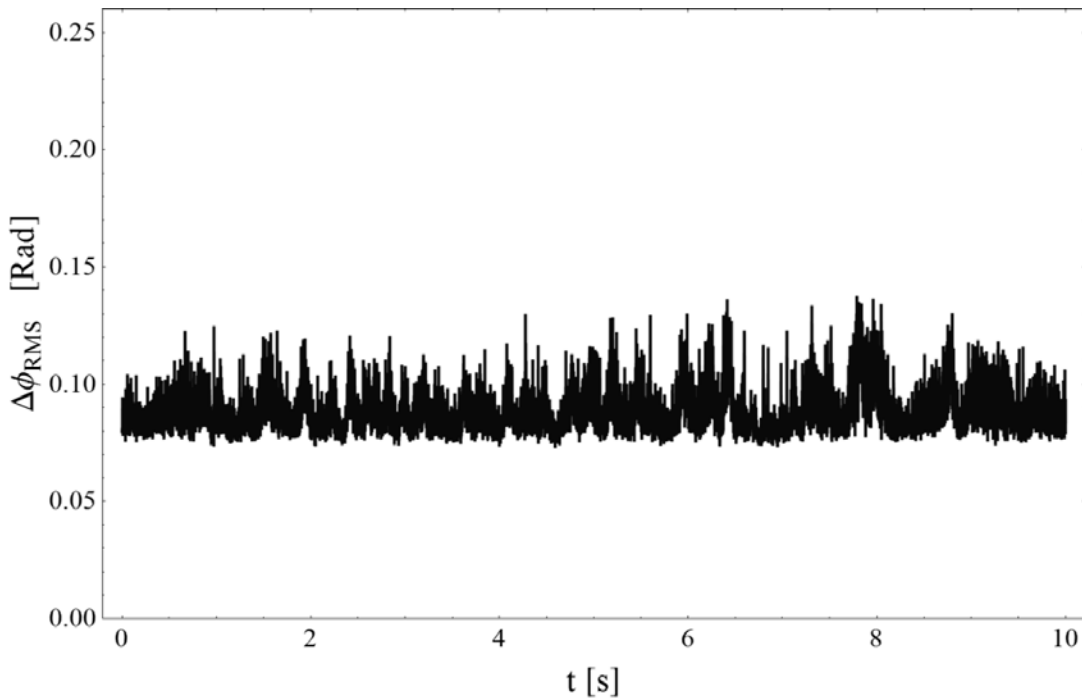


Figure 11: RMS phase error as a function of time for the 32 channel LOCSET system. RMS values calculated over a time period of 1ms with an average RMS phase error of $\lambda/71$ (~ 0.09 rad) [33].

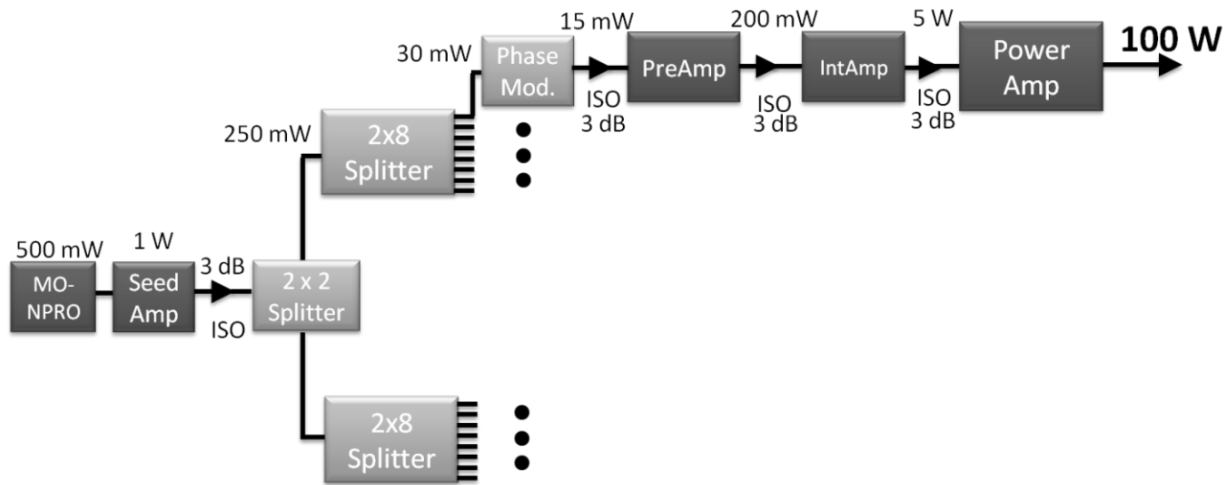
4. LOCSET High Power Beam Combining

The LOCSET technique is well established and coherent combination of 32 lasers at low power has been demonstrated. More importantly, the ability of LOCSET to potentially scale to hundreds of elements using a single photodetector is promising. Using electronic feedback to

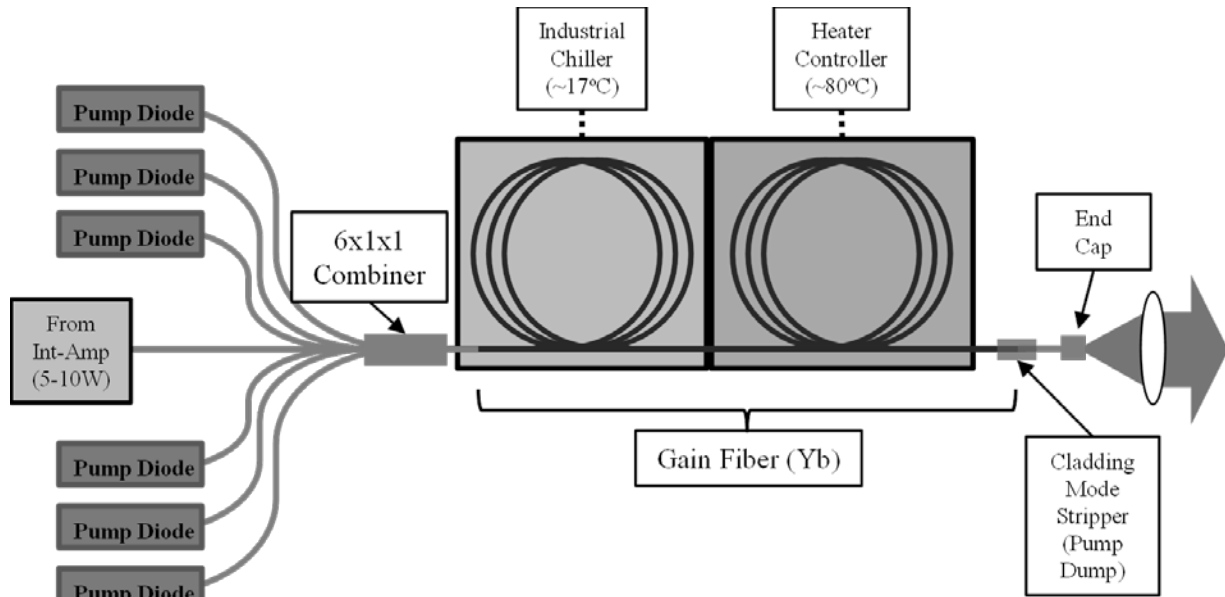
control the phases of the individual fiber amplifiers, we achieved an average rms phase stability of $\lambda/71$. In addition, LOCSET phase locking has been utilized by other researchers for beam combining applications, such as polarization beam combining [37], two-dimensional waveguide beam combining [38], remote target phase locking [39], and DOE beam combining (1D and 2D) [40,41]. Recently, to further demonstrate combining at higher powers, coherent combination of fiber amplifiers via LOCSET was extended into the kilowatt regime.

4.1 kW Scale Coherent Beam Combining of Silica Fiber Lasers

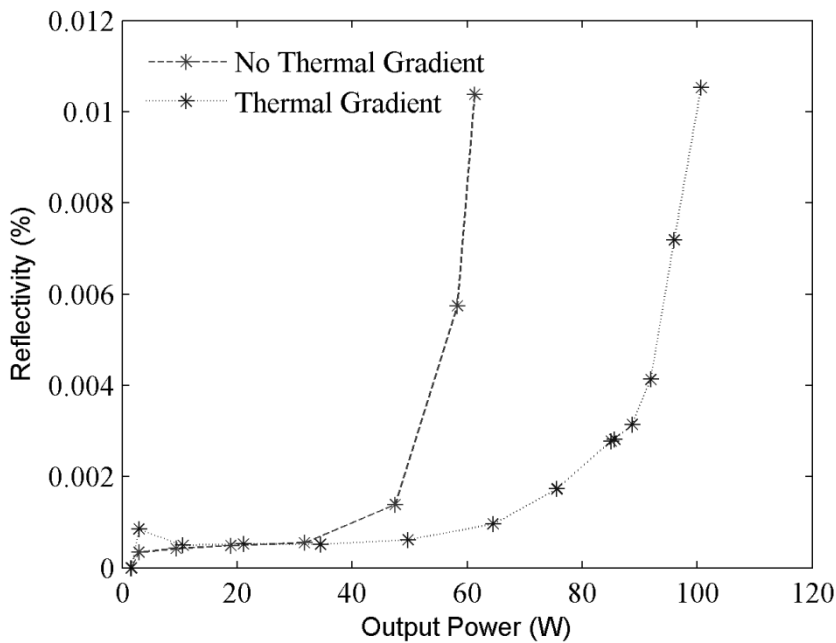
Coherent combination of sixteen 100 W single-frequency fiber amplifiers was investigated via LOCSET. Based on a standard MOPA configuration, a single-frequency Non-Planar Ring Oscillator (NPRO) was used to seed sixteen polarization maintaining (PM) fiber amplifiers. Each amplifier chain consisted of three fiber amplifier stages and produced 100 W of near diffraction limited ($M^2 \sim 1.1-1.2$) output power. A complete block diagram of the monolithic fiber amplifier chain for one element is shown in Figure 12a. In addition, a schematic of the Nufern co-pumped 100 W main amplifier is presented in Figure 12b. Here the power amplifier is seeded by the intermediate amplifier with 8 to 10 watts of 1064 nm light. Next, six 50 W (976 nm) fiber-coupled diode pump lasers (LIMO) were fusion spliced onto a 6x1x1 pump combiner. The ensuing output of the combiner is spliced onto a 5 meter long double clad PM Ytterbium (Yb) doped silica gain fiber, where the gain fiber is cladding pumped with the 976 nm light. While the pre-amplifier and intermediate gain stages are based on 6 μm (core)/125 μm (clad) and 10 μm /125 μm diameter gain fiber, respectively; the power amplifier stage uses a 25 μm /400 μm Nufern LMA fiber for SBS suppression.



(a)



(b)



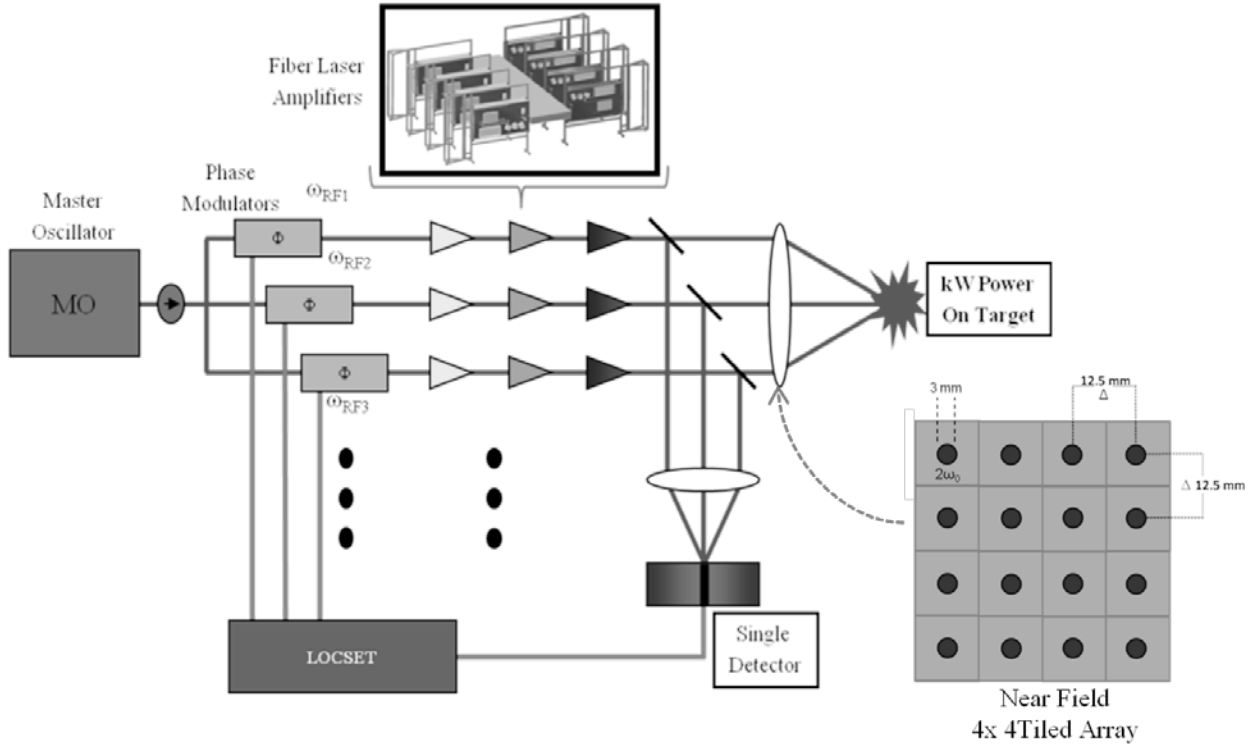
(c)

Figure 12: a) Block diagram of the monolithic fiber amplifier chain. b) Schematic of a co-pumped 100W fiber amplifier built by NuFern, SBS suppression accomplished via the introduction of a thermal gradient in the gain fiber with hot and cold fiber spools. c) Experimental reflectivity (%) vs. signal power for main amplifier with (dotted) and without (dashed) applied thermal gradient. Plot shows power enhancement via thermal gradient.

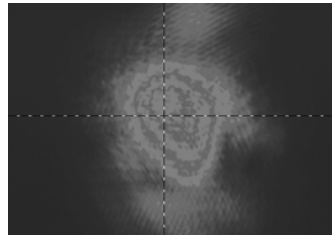
To further mitigate SBS, a two-stage thermal gradient was applied to the power amplifier, as shown in Figure 12b. SBS suppression can be achieved through utilization of the steep temperature gradient at the fiber output end [42] or application of an external thermal gradient, which applies a Brillouin frequency shift. Here the gain fiber is divided equally into two separate spools, a cold spool (17° C) and hot spool (80° C) held at constant temperature via thermoelectric coolers. A plot of the main amplifier backward power reflectivity versus signal output

power with (blue) and without (red) an applied thermal gradient is presented in Figure 12c. As expected, the thermal gradient provides a nearly two times enhancement in SBS threshold and allows us to reach 100 W of single-frequency power. Powers in excess of 100 W can be attained through shortening the fiber length, yet this is limited by increased unabsorbed pump powers and lower optical-to-optical efficiencies. Lastly, to maintain diffraction limited beam quality the fiber was coiled to suppress higher-order mode content [43]. A cladding mode stripper was also implemented to remove any unabsorbed (stray) pump cladding light. It is important to note that although 300 W of pump power is available, only 100 W of single-frequency power is achieved due to SBS limitations. Nevertheless, we can mitigate SBS by broadening the pump spectral linewidth. As such, we have recently utilized sinusoidal phase modulation to broaden the laser linewidth [44] and have attained pump-limited powers of >200 W at narrow linewidths (200 MHz).

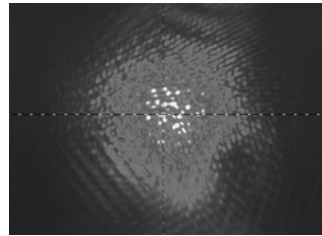
A fiber end cap was then added to the output fiber before diverging onto a collimating lens. After collimation (3-mm beam diameter), the sixteen output beams were directed onto external high-power isolators for optical return protection. However, due to moderate thermal lensing and astigmatic aberrations introduced by the isolators at high powers, the beam quality of the output fiber laser beams were slightly impaired (M^2 -1.2-1.3). A general schematic of the MOPA arrangement for the kW scale beam combination is shown in Figure 13a. The sixteen lasers were configured into a tiled 4 x 4 laser array where each beam was directed onto a far-field focusing lens by turning prisms. A self-referenced LOCSET scheme with 15 phase modulated beams and a single un-modulated reference beam was arranged. Subsequently, the sixteen beams were combined in the far-field where a 0.1% sampling wedge was used to sample the beam and direct it into a phase locking and beam diagnostic sub-system. Here the combined beam overlaps (interferes) onto the LOCSET photodetector and is further sampled into an imaging system. A re-imaging (magnification) system is used to enlarge the focal (combining) plane and optimize spatial overlap among all 16 beams. Lastly, a fast-photodiode is used to monitor the output intensity and estimate the RMS phase error.



(a)



(b)



(c)

Figure 13: Experimental arrangement for LOCSET CBC of 16 100 W lasers in a tiled 4x4 laser array ($2\omega_0 / \Delta = 0.24$). We note that the fill factor is limited by the size of the turning prisms, causing substantial power in the sidelobes. Resulting b) unlocked and c) phase locked beam profiles.

A total combined output power of 1.45 kW from the sixteen lasers was achieved with a residual phase fluctuation of $\lambda/25$. The resulting phase locked beam profiles are shown in Figures 13b and 13c, respectively. Unfortunately, the fill factor is limited by the size of our turning prisms ($D=12.5$ mm) and a low fill factor was attained ($2\omega_0 / \Delta = 0.24$). The ensuing low array fill factor results in substantial power in the side lobes. This can be remedied in future experiments by inserting longer focal length collimating lenses and expanding the beams for optimal subaperture fill factors of $2\omega_0 / D \sim 0.89$ [19]. Nevertheless, the phase locked beam profile exhibits a stable interference fringe pattern with amplified intensity; thereby confirming single-frequency kilowatt scale CBC of sixteen fiber lasers.

4.2 kW Scale Coherent Beam Combining of PCF amplifiers

Notably, kW scale beam combining was also attained with PCF amplifiers. In PCFs, micron-sized air holes in the cladding allow for precise control of the refractive index leading to larger core diameters while maintaining single mode operation. Another significant advantage of double-clad PCFs is the high numerical apertures that can be attained for pumping purposes through the utilization of a web of sub-wavelength silica bridges. Recently, novel SBS suppressive PCF amplifiers with 494 W of single-frequency [45] and 994 W of narrow linewidth (300 MHz) [46] output power, have been demonstrated. The PCF design is based on a segmented acoustic profile that is doped such that the core segments are optically uniform but acoustically inhomogeneous [45]. The acoustically modified PCF results in multiple Brillouin Gain Spectrum (BGS) peaks that help suppress SBS in single-frequency and narrow linewidth fiber lasers.

The acoustically manipulated fiber core, illustrated in Figure 14a, was designed to give two distinct Brillouin peaks. Here the Brillouin shift in the center region is comprised of one hexagon with different acoustic velocity, v_1 , than the acoustic velocity of the six outer regions, v_2 . In particular, a combination of dopants comprised of fluorine, aluminum, and germanium was used to achieve the segmentation of the acoustic index of refraction while maintaining uniformity of the optical index. To accommodate further SBS suppression through the application of externally applied or optically induced thermal gradients, the peaks were designed to have a separation of >200 MHz. Since the Brillouin shift is approximately 2 MHz/C° [47], this design would allow for the introduction of a temperature variation of $\sim 100 \text{ C}^\circ$ without overlap in the Brillouin gain bandwidth [45].

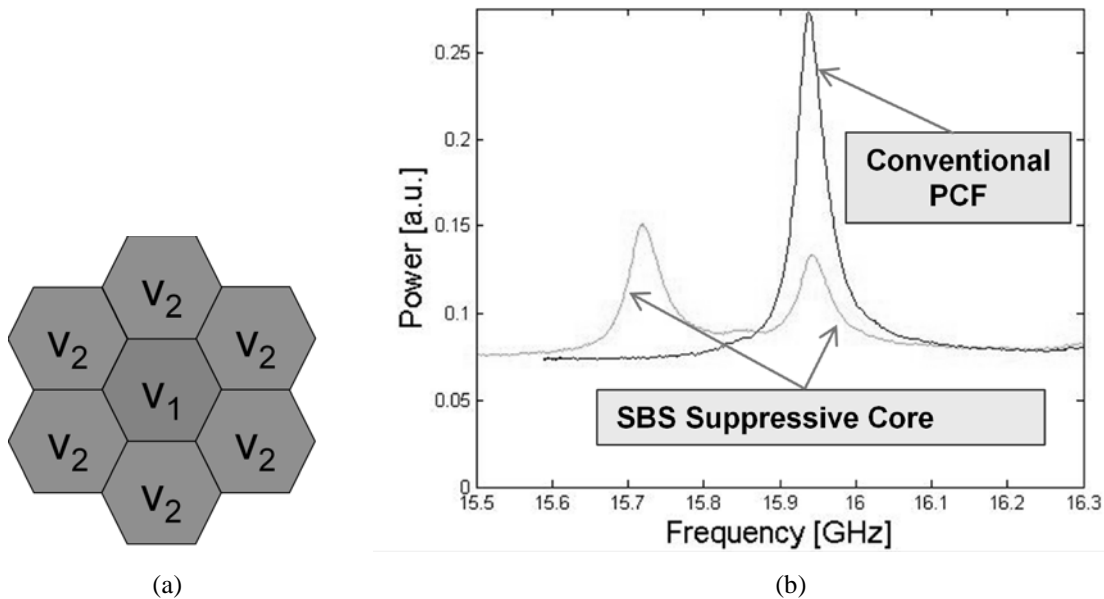


Figure 14: a) The core design of the segmented acoustic fiber. The Brillouin shift in the center region comprised of one hexagon is different than in the outer region comprised of six hexagons. b) BGS for acoustically segmented fiber confirming existence of two primary peaks. For comparison, the BGS for the reference fiber is shown [45].

A fiber based on the segmented acoustic design with a core diameter of $40 \mu\text{m}$ and mode field diameter (MFD) of $30 \mu\text{m}$ was fabricated by NKT Photonics. The inner cladding of the fiber was $300 \mu\text{m}$ with a nominal numerical aperture of 0.55-0.6. Furthermore, the pump absorption at 976 nm was estimated at 4 dB/m. Next, the BGS was investigated using a pump-probe technique. The resulting Brillouin spectrum, shown in Figure 14b, displays a shift of approximately 16

GHz two peaks with a separation of 220 MHz, as expected. Thereby, confirming the SBS suppression provided by the segmented acoustic PCF. Also shown is the BGS of a reference PCF, for the same pump and probe values. The reference fiber is a conventional PCF with identical core and cladding dimensions but no acoustic tailoring.

Subsequently, a high-power fiber amplifier was built around the segmented PCF. An experimental setup of the PCF amplifier arrangement with a counter-propagating pump scheme is depicted in Figure 15. Once again an NPRO was used as the master oscillator with the seed being amplified to 30 W using a three-stage amplifier system. This pre-amplifier was then free-space coupled into the core of the PCF amplifier with a 10 m long gain fiber. The pump power was provided by stacks of 976 nm Laserline diodes with a maximum output of 1.5 kW. Consequently, single-frequency output powers of up to 500 W were recorded without the onset of SBS [45]. Particularly, we were prevented from fully investigating the SBS suppressing characteristic of this amplifier by the sudden onset of modal instabilities [7]. Nonetheless, we have recently designed a PCF for concurrent SBS and modal instability suppression. The design utilizing simultaneous gain and acoustic tailoring led to the development of a 994 W narrow line (300 MHz), near-diffraction limited ($M^2 < 1.3$) PCF amplifier [46].

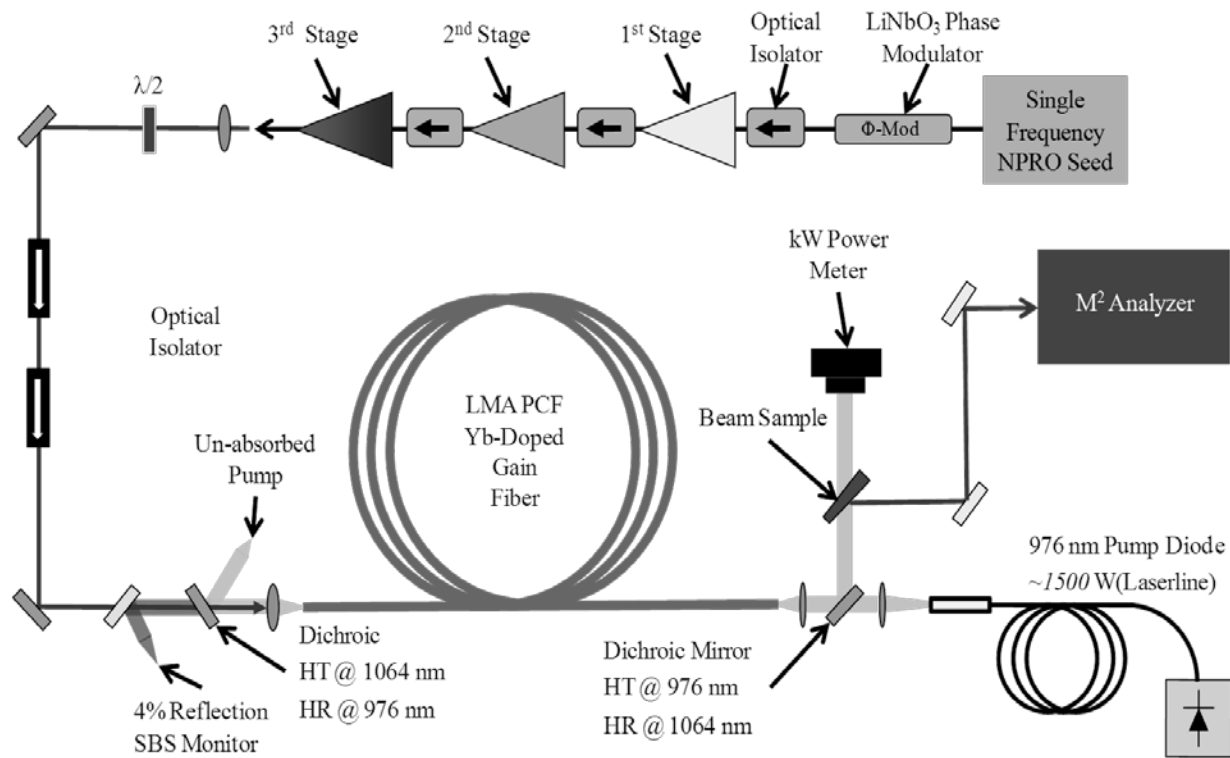


Figure 15: Experimental setup of counter-pumped PCF amplifier. A three stage amplifier system was utilized to provide approximately 30 W of seed power. Preamplifier seed and pump power were free-space coupled onto PCF amplifier.

Moreover, we analyzed the beam quality of the SBS suppressive amplifier. We conducted measurements using a Spiricon beam analyzer and M^2 values of less than 1.3 were obtained at all power levels. Based on this, it can be inferred that the development of an optical interface between segmented regions was minimal, if any. As a result, for the current experiments three ~400 W segmented acoustic fiber lasers were built and arranged in a filled aperture

configuration. Next, the beams were coherently combined through beam splitters and LOCSET phase electronics as shown in Figure 16. Ultimately, the 3-element beam combination experiments resulted in 1.04 kW of combined power with a residual phase fluctuation of $\lambda/18$. Intensity and beam profile measurements are shown in Figures 17a and 17b, respectively. Notably, the filled aperture arrangement results in 1 kW of power in a single central lobe, with near diffraction limited beam quality. Hence, single-frequency kW beam combining via LOCSET has been demonstrated with both conventional silica and novel SBS suppressive PCF fiber lasers.

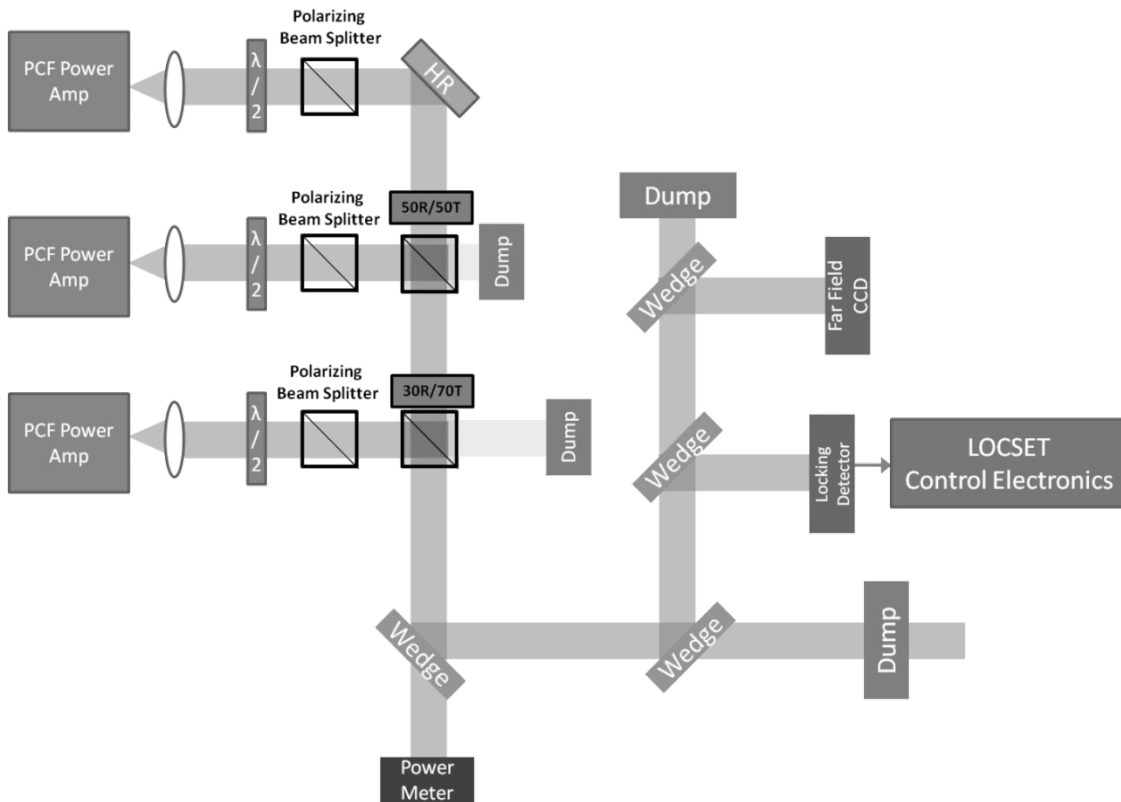


Figure 16: Single-frequency combination of three 400 W PCF amplifiers in a filled aperture CBC arrangement. LOCSET phase locking is used to coherently combine the lasers and produce 1 kW of power.

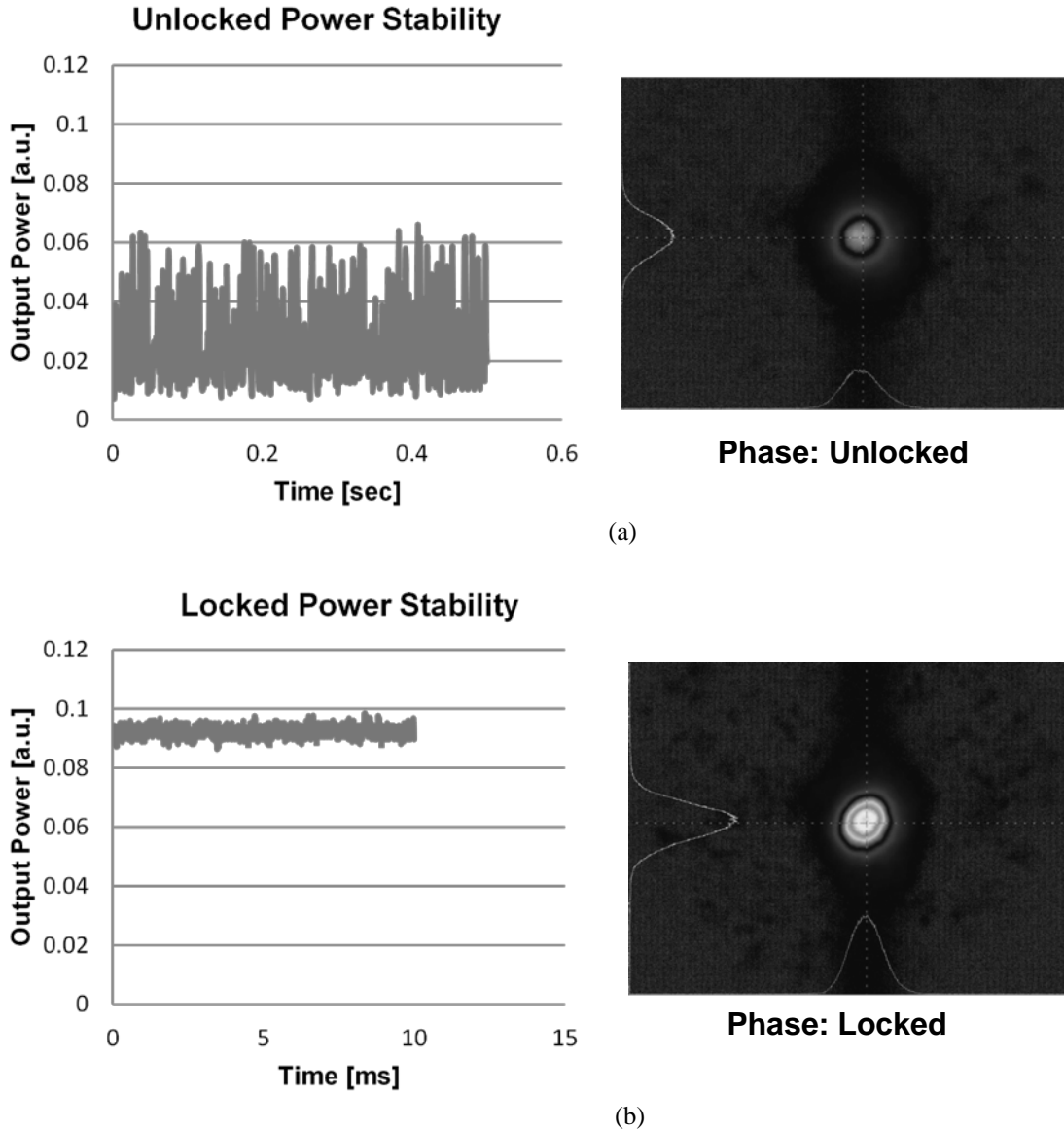


Figure 17: Beam combination time-varying intensity (left) and beam profile (right) of three PCF amplifiers a) unlocked and b) phase locked via LOCSET.

High power single-frequency laser sources with good beam quality are highly desired due to their utility in coherent beam combining, gravitational wave detection [48], and nonlinear frequency conversion [49]. In terms of CBC, single-frequency beam combining circumvents path-length matching techniques required to combine narrow linewidth high-power fiber lasers. Here single-frequency lasers denote lasers with linewidths smaller than the Brillouin linewidth (~ 60 MHz) and narrow line fiber lasers refer to lasers with gigahertz wide spectral widths. Regardless, LOCSET beam combining should effortlessly extend to narrow linewidth beam combining as long as path length matching tolerances are met. As such, we have recently demonstrated LOCSET beam combining at narrow linewidths with sinusoidal phase modulation [44].

5. Conclusion

Fiber lasers have superior beam quality, size, weight, and efficiency advantages over conventional solid state and chemical lasers. Although constrained by power scaling limits of individual fibers, beam combination of multiple fiber lasers can overcome such drawbacks. Towards that end, LOCSET is an established phase locking technique that has been used for coherent fiber laser beam combination. Notably, the recent high power experiments in both tiled (conventional silica fiber) and filled aperture (PCF) arrangements establish LOCSET's viability at kilowatt power levels, with as many as sixteen high-power lasers (100 W) coherently combined. In addition, LOCSET's channel scalability and error performance was analyzed through low power multi-channel LOCSET CBC of 2, 16, and 32 channels. Here 32 channel LOCSET beam combining with excellent RMS phase error of $\lambda/71$ was reported [33]. More importantly, there was no phase error degradation when scaling from 2 channels to 32 channels, as expected from previous simulations [17]. Furthermore, due to LOCSET's high operational bandwidth and low phase error, LOCSET appears readily scalable for efficient combination of over 100 lasers.

References

- [1] L. Quintino, A. Costa, R. Miranda, D. Yapp, V. Kumar, and C. J. Kong, "Welding with high power fiber lasers – A preliminary study," *Materials & Design* **28**, 1231-1237 (2007).
- [2] S. D. Jackson and A. Lauto, "Diode-pumped fiber lasers: A new clinical tool?," *Lasers in Surgery and Medicine* **30**, 184-190 (2002).
- [3] P. Sprangle, J. Peñano, B. Hafizi, and A. Ting, "Incoherent Combining of High-Power Fiber Lasers for Long-Range Directed Energy Applications," *Journal of Directed Energy* **2**, 273-284 (2007).
- [4] R. G. Smith, "Optical power handling capacity of low loss optical fibers as determined by stimulated Raman and Brillouin scattering," *Applied Optics* **11**, 2489-2494 (1972).
- [5] E. Lichtman, R. G. Waarts and A. A. Friesem, "Stimulated Brillouin scattering excited by a modulated pump wave in single-mode fibers", *J. Lightwave Technology* **7**, 171-173 (1989).
- [6] B. Ward, C. Robin, and I. Dajani, "Origin of thermal modal instabilities in large mode area fiber amplifiers," *Opt. Express* **20**, 11407-11422 (2012).
- [7] A. V. Smith and J. J. Smith, "Mode instability in high power fiber amplifiers," *Optics Express* **19**, 10180-10192 (2011).
- [8] P. Sprangle, J. Peñano, B. Hafizi, and A. Ting, "Incoherent Combining of High-Power Fiber Lasers for Long-Range Directed Energy Applications," *Journal of Directed Energy* **2**, 273-284 (2007).
- [9] S. J. Augst, T. Y. Fan, "Coherent beam combining and phase noise measurements of ytterbium fiber amplifiers," *Optics Letters* **29**, 474-476 (2004).
- [10] P. Sprangle, A. Ting, J. Penano, R. Fischer, and B. Hafizi, "Incoherent combining and atmospheric propagation of high-power fiber lasers for directed-energy applications," *IEEE Journal of Quantum Elec.* **45**, 138-148 (2009).
- [11] C. Wirth, O. Schmidt, I. Tsybin, T. Schreiber, R. Eberhardt, J. Limpert, A. Tünnermann, K. Ludewigt, M. Gowin, E. ten Have, and M. Jung, "High average power spectral beam combining of four fiber amplifiers to 8.2 kW," *Optics Letters* **36**, 3118-3120 (2011).
- [12] P. Madasamy, D. R. Jander, C. D. Brooks, T. H. Loftus, A. M. Thomas, P. Jones, and E. C. Honea, "Dual-grating spectral beam combination of high-power fiber lasers," *IEEE Journal of Sel. Top. In Quan. Elec.* **15**, 337-343 (2009).
- [13] E. J. Bochove and S. A. Shakir, "Analysis of a spatial-filtering passive fiber laser beam combining system," *IEEE Journal of Sel. Topics in Quant. Elect.* **15**, 320-327 (2009).
- [14] C. J. Corcoran, F. Durville, K. A. Pasch, and E. J. Bochove, "Spatial filtering of large mode area fiber lasers using a self-Fourier cavity for high power applications," *Journal of Optics A* **9**, 128-133 (2007).
- [15] J. Rothenberg, "Passive coherent phasing of fiber laser arrays," *Proceedings of SPIE* **6873**, 687315 (2008).
- [16] Jérôme Bourderionnet, Cindy Bellanger, Jérôme Primot, and Arnaud Brignon, "Collective coherent phase combining of 64 fibers," *Optics Express* **19**, 17053-17058 (2011).

- [17] T. M. Shay, "Theory of electronically phased coherent beam combination without a reference beam," *Optics Express* **14**, 12188-12195 (2006).
- [18] D. C. Jones, A. M. Scott, S. Clark, C. Stace, and R. G. Clarke, "Beam steering of a fibre bundle laser output using phased array techniques," *Proceedings of SPIE* **5335**, 125-131 (2004).
- [19] M. A. Vorontsov and S. L. Lachinova, "Laser Beam Projection with Adaptive Array of Fiber Collimators. I. Basic Considerations for Analysis," *Journal of Optical Society of America A* **25**, 1949-1959 (2008).
- [20] H. Bruesselbach, S. Wang, M. Minden, D. C. Jones, and M. Mangir, "Power scalable phase-compensating fiber-array transceiver for laser communications through atmosphere," *Journal of Optical Society of America B* **22**, 347-353 (2005).
- [21] A. Flores, T. M. Shay, C. A. Lu, C. A. Robin, B. Pulford, A. D. Sanchez, D. Hult, and K. Rowland, "Coherent Beam Combining of Fiber Amplifiers in a kW Regime," *Conference on Lasers and Electro-Optics -CLEO 2011*, Baltimore, MD, CFE3.
- [22] C. X. Yu, S. J. Augst, S. M. Redmond, K. C. Goldizen, D. V. Murphy, A. Sanchez, and T. Y. Fan, "Coherent combining of a 4 kW, eight-element fiber amplifier array," *Optics Letters* **36**, 2686-2688 (2011).
- [23] S. M. Redmond, T. Y. Fan, D. Ripin, P. Thielen, J. Rothenberg, and G. Goodno, "Diffractive Beam Combining of a 2.5-kW Fiber Laser Array," in *Lasers, Sources, and Related Photonic Devices*, paper AM3A.1 (2012).
- [24] T. H. Loftus, A. M. Thomas, M. Norsen, J. Minelly, P. Jones, E. Honea, S. A. Shakir, S. Hendow, W. Culver, B. Nelson, and M. Fitelson, "Four-Channel, High Power Passively Phase Locked Fiber Array," *Advanced Solid-State Photonics 2008*, WA4 (2008).
- [25] G.D. Goodno, C.P. Asman, J. Anderegg, S. Brosnan, E.C. Cheung, D. Hammons, H. Injeyan, H. Komine, W. H. Long, M. McClellan, S. J. McNaught, S. Redmond, R. Simpson, J. Sollee, M. Weber, S.B. Weiss, and M. Wickham, "Brightness-Scaling Potential of Actively Phase-Locked Solid-State Laser Arrays," *IEEE Journal of Sel. Top. In Quan. Elec.* **13**, 460-472 (2007).
- [26] J. Anderegg, S. Brosnan, E. Cheung, P. Epp, D. Hammons, H. Komine, M. Weber and M. Wickham, "Coherently coupled high-power fiber arrays", *Proceedings of SPIE* **6102**, 61020U (2006).
- [27] M. A. Vorontsov, G. W. Carhart, and J. C. Ricklin, "Adaptive phase-distortion correction based on parallel gradient-descent optimization," *Optics Letters* **22**, 907-909 (1997).
- [28] L. Liu, M.A. Vorontsov, E. Polnau, T. Weyrauch and L.A. Beresnev, "Adaptive phase-locked fiber array with wavefront phase tip-tilt compensation using piezoelectric fiber positioners", *Proceedings of SPIE* **6708**, 67080K (2007);
- [29] T.M. Shay, V. Benham, J.T. Baker, A.D. Sanchez, D. Pilkington, and C.A. Lu, "Self-Synchronous and Self-Referenced Coherent Beam Combination for Large Optical Arrays," *IEEE Journal of Sel. Top. in Quan. Elec.* **13**, 480-486 (2007).
- [30] T. M. Shay, J. T. Baker, A. D. Sanchez, C. A. Robin, C. L. Vergien, A. Flores, C. Zerinque, D. Gallant, C. A. Lu, B. Pulford, T. J. Bronder, and A. Lucero, "Phasing of High Power Fiber Amplifier Arrays," *Advanced Solid-State Photonics*, paper AMA1 (2010).
- [31] G. Goodno, S. McNaught, J. Rothenberg, T. McComb, P. Thielen, M. Wickham, and M. Weber, "Active phase and polarization locking of a 1.4 kW fiber amplifier," *Optic Letters* **35**, 1542-1544 (2010).
- [32] C. X. Yu, J. E. Kinsky, S.E.J. Shaw, D. V. Murphy, and C. Higgs, "Coherent beam combining of large number of PM fibers in 2-D fiber array," *Electronic Letters* **42**, 1024-1025 (2006).
- [33] B. Pulford. *LOCSET Phase Locking: Operation, Diagnostics, and Applications*. Dissertation, University of New Mexico (2011).
- [34] G.D. Goodno, C. Shih, and J.E. Rothenberg, "Perturbative analysis of coherent combining efficiency with mismatched lasers," *Optics Express* **18**, 25403-25414 (2010).
- [35] D.C. Jones, C.D. Stacey, and A.M. Scott, "Phase stabilization of a large-mode-area ytterbium-doped fiber amplifier," *Optics Letters* **32**, 466-468.
- [36] B. Pulford, "32 Channel LOCSET Coherent Beam Combining," manuscript to be submitted (2012).
- [37] R. Uberna, A. Bratcher, B.G. Tiemann, T.G. Alley, A.D. Sanchez, A. Flores, and B. Pulford, "Coherent polarization beam combination with active phase and polarization control," *Solid State and Diode Laser Technology Review (SSDLTR) Technical Digest*, 12-16 (2010).
- [38] R. Uberna, A. Bratcher, T.G. Alley, A.D. Sanchez, A. Flores, and B. Pulford, "Coherent combination of high power fiber amplifiers in a two-dimensional re-imaging waveguide," *Optics Express* **18**, 13547-13553 (2010).
- [39] V. Jolivet, P. Bourdon, B. Bennai, L. Lombard, D. Goular, E. Pourtal, G. Canat, Y. Jaoeun, B. Moreau, and O. Vassuer, "Beam Shaping of Single-Mode and Multimode Fiber Amplifier Arrays for Propagation Through Atmospheric Turbulence," *IEEE Journal of Sel. Top. In Quan. Elec.* **15**, 257-268 (2009).

- [40] M. Wickham, P. Thielen, J. Jo, G. Goodno, R. Rice, E. Cheung, J. Rothenberg, D. Gallant, J. Baker, A. Lucero, A. Sanchez, T. Shay, C. Robin, C. Vergien, and C. Zeringue, "High efficiency coherent fiber beam combiner," *2008 Annual Directed Energy Symposium Proceedings*.
- [41] P. Thielen, J. Ho, D. Burchman, G. Goodno, J. Rothenberg, M. Wickham, A. Flores, C. Lu, B. Pulford, C. Robin, A. Sanchez, D. Hult, and K. Rowland, "Two-Dimensional Diffractive Coherent Beam Combining," in *Advanced Solid-State and Photonics (ASSP) 2012*, paper AM3A.2.
- [42] Y. Jeong, J. Nilsson, J. K. Sahu, D. N. Payne, R. Horley, L. M. B. Hickey, and P. W. Turner, "Power scaling of single-frequency ytterbium-doped fiber master oscillator power amplifier sources up to 500 W," *IEEE J. Sel. Top. Quantum Electron.* **13**, 546-551 (2007).
- [43] J. P. Koplav, D. Kliner, and L. Goldberg, "Single-mode operation of a coiled multimode fiber amplifier," *Optics Letters* **25**, 442-444 (2000).
- [44] A. Flores, C. Lu, C. Robin, and I. Dajani, "Experimental and theoretical studies of phase modulation in Yb-doped fiber amplifiers," *Proceedings of SPIE* **8281**, 83811B (2012).
- [45] C. Robin and I. Dajani, "Acoustically segmented photonic crystal fiber for single-frequency high-power laser applications," *Optics Letter* **36**, 2641-2643 (2011).
- [46] C. Robin, I. Dajani, C. Zeringue, B. Ward, and A. Lanari, "Gain-tailored SBS suppressing photonic crystal fibers for high power applications," *Proceedings of SPIE* **8237**, 82371D (2012).
- [47] M. Hildebrandt, S. Büesche, P. Weßels, M. Frede, and D. Kracht, "Brillouin scattering spectra in high-power single-frequency ytterbium doped fiber amplifiers," *Optics Express* **16**, 15970-15979 (2008).
- [48] D. Kracht, R. Wilhelm, M. Frede, C. Fallnich, F. Seifert, B. Willke, and K. Danzmann, "High power single-frequency laser for gravitational wave detection," in *Advanced Solid-State Photonics*, paper WE1 (2006).
- [49] F.J. Kontur, I. Dajani, Y. Lu, and R.J. Knize, "Frequency-doubling of a CW fiber laser using PPKTP, PPMgSLT, and PPMgLN," *Optics Express* **15**, 12882-12889 (2007).

DISTRIBUTION LIST

DTIC/OCP 8725 John J. Kingman Rd, Suite 0944 Ft Belvoir, VA 22060-6218	1 cy
AFRL/RVIL Kirtland AFB, NM 87117-5776	1 cy
Angel Flores Official Record Copy AFRL/RDLT	1 cy